

TECHNICAL UNIVERSITY OF DENMARK (DTU)

MASTER THESIS

MSC. ENG. SUSTAINABLE ENERGY

Assessment of solar energy in Greenland: Analyzing potential and resource availability



FEDERICO BASILE - s233116

SUPERVISORS:

ADAM RASMUS JENSEN
IOANNIS SIFNAIOS
JANNE DRAGSTED

Contents

Acknowledgements	iii
AI Assistance Statement	iv
1 Introduction	1
1.1 Current status of solar power in Greenland	3
1.2 Objectives	3
2 Solar resource data	5
2.1 Measurement data	5
2.1.1 DMI data	5
2.1.2 Asiaq data	8
2.1.3 Quality control of the DMI data	8
2.2 Modeled data	15
2.2.1 ERA5 data	15
2.2.2 NASA POWER data	15
2.3 Data validation	15
3 PV energy potential	20
3.1 Modeling a PV plant	20
3.1.1 Albedo	22
3.1.2 Clear sky model	23
3.1.3 Bifaciality	23
3.2 Electricity consumption data description	23
3.3 Simulate PV production	25
3.3.1 Snow coverage of the PV panels	25
4 Results	27
4.1 Bifacial panels, tilted by 60°	27
4.2 Vertical bifacial panels	31
4.3 Monofacial panels	35
4.4 Emissions reduction	39
4.4.1 Emission factor	39
4.4.2 Saved emissions results and discussion	39
4.4.3 Potential for electric heating	41
5 Conclusion	43
A Hydropower plants	I
B Example of time step distribution for the Nuuk station	II
C 2-D visualizations	II

D Additional data filtering	IV
E Scatter plots	V
F Location of the settlements of interest	X
G Energy consumption in Ilimanaq and Qeqertarsuatsiaat	XI
H PV Production	XII
H.1 Bifacial panels, 60° tilt	XII
H.2 Bifacial panels, 45° tilt	XIII
H.3 Vertical bifacial panels	XVII
H.4 Monofacial panels, 40° tilt	XIX

Acknowledgements

I would like to express my sincere gratitude to my supervisor, Adam Rasmus Jensen, and my co-supervisors, Ioannis Sifnaios and Janne Dragsted, for providing invaluable guidance, feedback, and support throughout the development of this thesis. Their expertise and encouragement have been fundamental in shaping the direction and quality of this work.

A special thanks goes to Esben Lundø Madsen, from Nukissiorfiit, and to Tove Lading, Associate Professor at the Department of Civil and Mechanical Engineering at DTU, for the help they gave me by providing very precious data and insights that greatly enriched my research.

Finally, I am grateful to the Department of Wind and Energy Systems at DTU for providing the academic environment and resources that made this research possible..

AI Assistance Statement

This thesis has benefited from the use of AI tools, particularly OpenAI's ChatGPT, for language refinement, code debugging, and assistance in literature and report structuring. All content has been critically reviewed and adapted by the author to ensure technical accuracy and academic integrity.

1 Introduction

Climate change affects every environment of the world, with the main effect being a global temperature rise of 1.1 °C since 1880, marked as the start of modern industrialization, and there is an 80 percent likelihood that this amount will exceed 1.5°C before 2030. [1]

A NASA study [2] also confirms that not all the areas of Earth are equally affected by the phenomenon: in 2022 some Arctic regions, for example, experienced a temperature anomaly higher than 4°C than the 1951-1980 average. Polar regions are also subject to positive feedback mechanisms, physical phenomena that speed up the ice melting and consequently the rise of temperatures like the albedo effect (as ice melts, it exposes darker ocean or land, which absorbs more sunlight, causing further warming and more ice melt) or an increased water vapor effect, since more ocean surface leads to more evaporation and eventually to higher amounts of H₂O in the atmosphere.

The result of these factors combining together is that the Arctic has been warming almost four times faster than the rest of the world in the last 50 years [3], and such a number testifies the destroying impact that global warming has on these areas of the world.

It is in the scope of this project to study how the Arctic region can be part of the global effort against climate change.

Greenland, in particular, is the world's largest island excluding continental islands, with an area of 2.2 million square kilometers and 57'000 inhabitants living in 190 towns and settlements along the coast and whose surface is 82% covered by ice sheet and whose temperature increase keeps accelerating. [4] [5]

Because of its geographical position, Greenland is highly depending on fossil fuels: 83% of the island's primary energy demand, as of 2019, was constituted by oil, while only 16% is made by hydropower. [6] These values change when looking at electricity generation, where renewables account for around 78% of the total, almost completely thanks to hydropower.

Hydropower generation takes place at five power plants (Nuuk, Tasiilaq, Paakitsoq, Qorlortorsuaq and Sisimiut) which have a total capacity of 91MW [7]. Their location on the island can be seen in the Appendix A.

The non-renewable share is composed by diesel-powered electricity generators, which are the main and only electric power source in small settlements. [8]

This happens because Greenlandic energy supply is characterized by island operation: the distance between towns and the harsh weather conditions of the territory make electrical connections and infrastructures difficult to build, meaning that the isolated villages can't be reached and must rely on localized solutions.

Nukissiorfiet is the Greenlandic government-owned energy company: they are responsible for most of the island's electricity, water and heat supply, and they own the already mentioned hydroelectric power plants. They serve 17 towns and 53 settlements, although leaving 5 towns and 67 settlements unsupplied, relying on fossil fuels.

Renewable energy is a relatively recent addition to the Greenlandic energy system, as hydropower was only introduced in 1993. Before then, fossil fuels were the only component of the island's energy mix, including gas oil, Diesel Fuel Artic (often referred to as DFA), gasoline, petroleum, and other minor

fuels, with gas oil and DFA representing the vast majority of the consumption share.

Gas oil is also the fuel utilized by Nukissiorfiit for electricity production in their district and urban combined heat and power plants (CHP) and by power plants in settlements; these two last solutions however represent the minority of the electricity production. In 2023, out of the 2'101 TJ of electricity produced by Nukissiorfiit, 1'729 were generated by hydropower plants, and the remaining share was split between CHP and settlements plants. [9]

The increasing share of hydropower led to an overall reduction in GHG emissions of the island for energy consumption, which decreased by 2.5% from 1990 to 2023, when the total amounted to 605 thousands tons of CO₂eq, as Figure 1 shows. A peak was reached in 2010 and 2011 due to the execution of three and five oil exploration wells off West Greenland, when the figure was slightly higher than 700 thousands tons of CO₂eq, before a fast drop in the immediately following years, when the mentioned operation ceased. Since then, a slower but steady increase was registered until 2023.

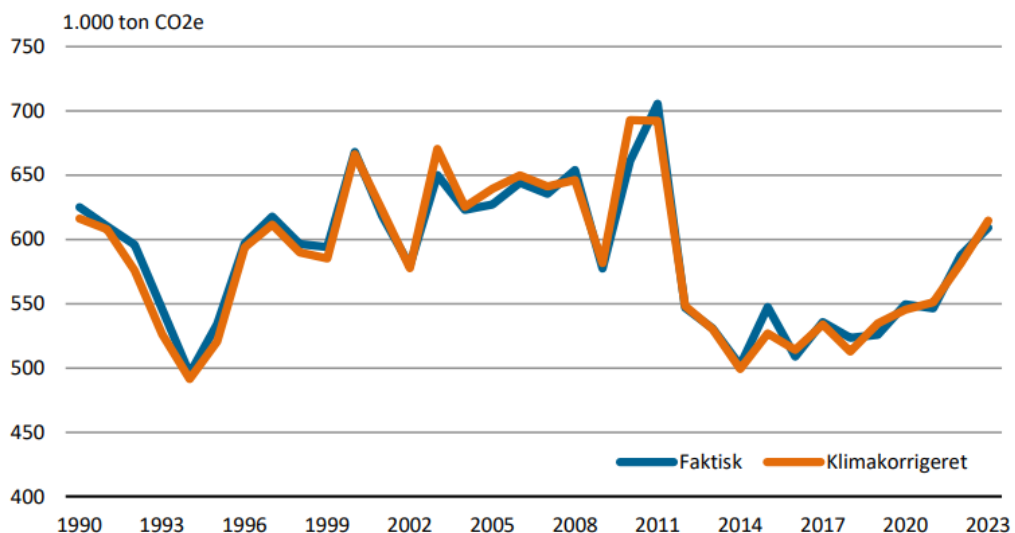


Figure 1: Emission of greenhouse gases from energy consumption in Greenland, 1990-2023 [9]

A more encouraging trend is observable in Figure 2, reporting the emission of greenhouse gases per fuel unit. The effect of renewable energy is visible in the continuously decreasing trend that Greenland experienced in the 1990-2023 period, with the figure dropping from 74 to 61 kg of GHG per GJ of energy consumed, corresponding to a 16.7% decrease over the mentioned time span.

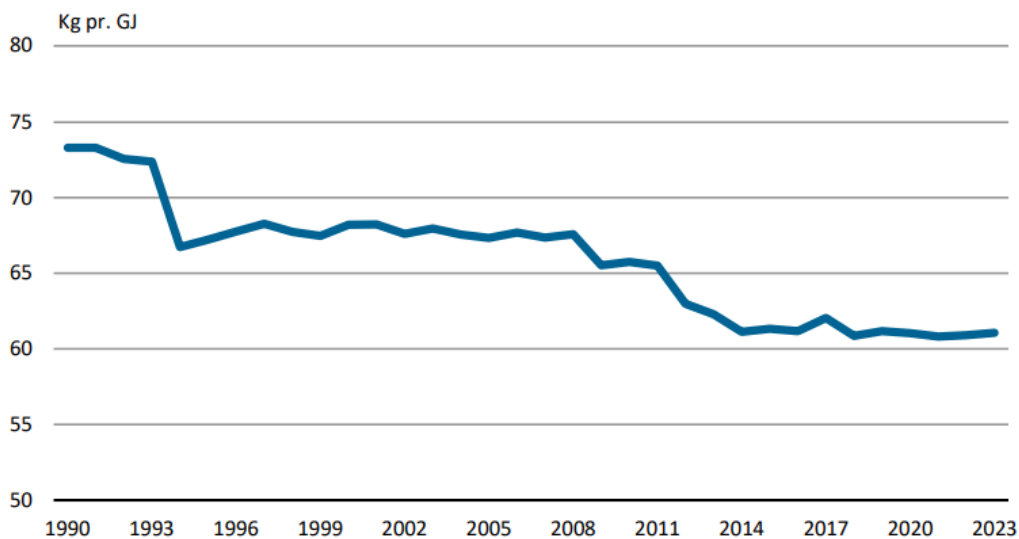


Figure 2: Emission of greenhouse gases per fuel unit in Greenland, 1990-2023 [9]

1.1 Current status of solar power in Greenland

As mentioned earlier, 78% of electricity generation in Greenland comes from renewable sources, with a vast dominance of hydropower. Hydropower constitutes 97% of the total renewable generation, with the remaining 3% coming from wind, solar, bioenergy, and geothermal.

From these values it is clear how solar is yet to be a reliable and widespread energy source: indeed, as of October 2024, there are 162 registered PV systems in Greenland with a combined capacity of 2 MWp: 146 of them are privately owned, and the majority of them are roof-mounted system with a capacity between 4 and 12 kWp. Nukissiorfít owns the remaining 16 PV systems, with a total capacity of 620kWp.

The potential of a wider PV implementation is concentrated in the spring and summer months, when in Greenland benefits from extended daylight hours and, above certain latitudes, the midnight sun phenomenon, also known as the polar day, occurs: due to the high latitudes of the island, the sun doesn't go below the horizon for many days. It involves all the locations of the northern hemisphere above 65°44'N.

The length of the midnight sun varies with the location: in Sisimiut, located at 66°N, just above the Arctic Circle, the sun does not set from the 3rd of June to the 11th of July, while in Qaanaaq, at 77°N, the period is much longer, spanning from the 21st of April to the 23rd of August. Such a prolonged absence of the night, creates the perfect conditions for an implementation of photovoltaic systems in Greenland.

1.2 Objectives

This thesis aims to understand how Greenland's carbon footprint will be affected by a greater implementation of photovoltaic solutions on its territory.

To do so, the thesis will first move from the obtainment of a solar resource ground measurement

dataset for Greenlandic locations, based on what sources are made available from weather entities (DMI, the Danish Meteorological Institute and/or Asiaq, the Greenlandic weather institution), which will consequently be analyzed, quality checked, filtered and cleaned, in order to eliminate imperfections and have a dataset as coherent to reality as possible.

Subsequently, two reanalysis datasets' sources (ERA5 and NASA POWER) will be taken into consideration and compared to the filtered and cleaned measurement dataset to assess, via statistical analysis, which of them is more adherent to reality and can be thereby chosen as reference source for the further steps of the analysis.

The preferred dataset will then be used as the source to simulate the performance and energy production of a Python-modeled photovoltaic plant built in Ililamaaq, a settlement in Western Greenland of which consumption data for the year 2023 has been provided by Nukissiorfiit, via personal communication with the information owner.

A detailed analysis of the inputs needed by the model to obtain the resulting AC energy outputs will be undertaken, to explain and understand the reasons behind the choice of required parameters.

The simulations will be run for both mono- and bifacial panels, with different tilts and orientations and its results will be compared to the consumption data in order to compute displaced energy, curtailed energy and solar contribution for every scenario. Monofacial modules aim to recreate roof-mounted systems, while bifacial panels are the technology that this study assumes to be using in ground-mounted PV plants.

Using an emission factor calculated and published by Nukissiorfiit [10], the saved CO₂ quantities will be computed for all the different cases and a further analysis of the results, taking all the mentioned factors into consideration, will be conducted for suggesting realistic emission reduction opportunities for Ililamaaq and the whole Greenland.

2 Solar resource data

To test the impact photovoltaic can have on the Greenlandic energy mix it is necessary to start with the solar radiation data gathering. The solar resource has three main components:

- DNI: Direct Normal Irradiance, or Beam, is the component of solar radiation hitting a surface perpendicular to the sun rays;
- DHI: Diffuse Horizontal Irradiance, is the component of solar radiation scattered by the atmosphere before reaching the ground. It comes from every direction and is divided into isotropic, circumsolar, and horizon diffuse;
- GHI: Global Horizontal Irradiance, is the sum of cosine corrected direct and diffuse irradiance and refers to an horizontal surface. Calling θ_z the zenith angle, complementary to the solar elevation angle, GHI is calculated as follows:

$$GHI = DHI + DNI \cdot \cos(\theta_z) \quad (1)$$

- G_R : Ground Reflected Irradiance is the total ground-reflected irradiance incident on a surface and is always equal to zero for horizontal surfaces;
- G_{POA} : Global Plane of Array Irradiance, is the irradiance hitting the solar panel with a general tilt angle β , and takes into account the beam, diffuse and reflected components.

The first stage of the project is to identify and retrieve GHI data from online sources and compare the different versions to validate them and have a reliable dataset to operate with.

2.1 Measurement data

Ground measurement provides the most accurate data in terms of proximity to the actual irradiance value. Moreover, measurement data can be made at a very high temporal resolution.

The two identified measurement data sources for solar irradiance in Greenland were the Danish Meteorological Institute (Danmarks Meteorologiske Institut - DMI) and Asiaq, a Greenlandic research institute based in Nuuk.

2.1.1 DMI data

Greenlandic weather data is made publicly available by the Danish Meteorological Institute through APIs, which allows the download of several parameters including ground-measured GHI.

DMI owns 252 weather stations in Greenland but only 6 of them measure global radiation.

Table 1 reports the details of these stations.

Table 1: DMI weather stations providing global radiation data.

Station name	Latitude	Longitude	Data available from	Status
Nuuk	64.175	-51.736	2007-06-08	Active
Aasiaat	68.708	-52.852	2009-10-12	Active
Narsarsuaq	61.158	-45.440	2012-09-25	Active
Ittoqqortoormiit	70.484	-21.951	2005-08-25	Active
Tasiilaq	65.611	-37.637	2005-08-23	Active
Danmarkshavn	76.769	-18.668	2010-05-22	Active

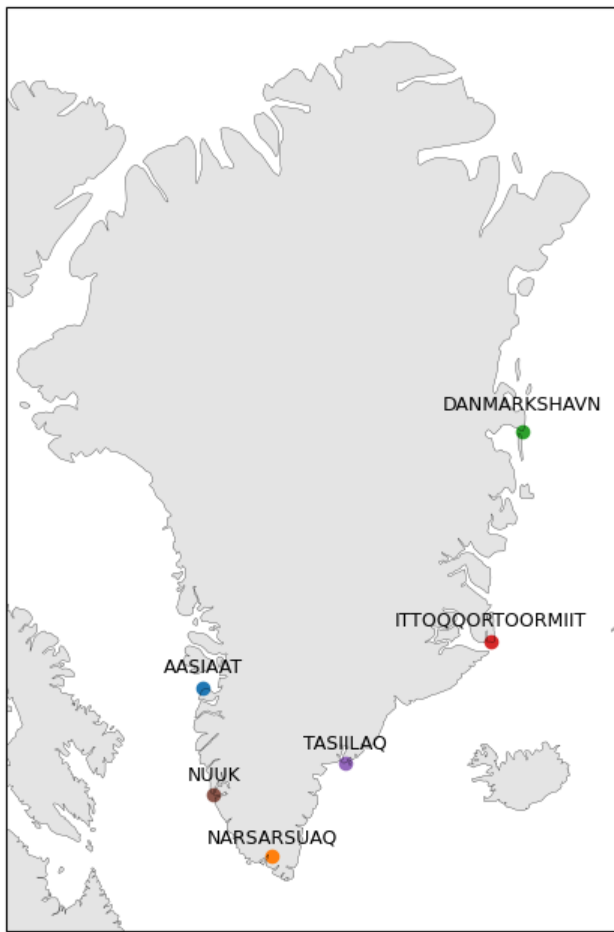


Figure 3: Map of the DMI meteorological stations with irradiance data

The data is provided in W/m^2 , and reports, quoting the DMI website, the latest 10 minutes global radiation mean intensity. Despite the website description, not all the data is provided with a time step of 10 minutes: from Appendix B it is possible to see how, in particular for early years, the resolution is mainly hourly, becoming predominantly a 10-minute resolution from 2014 on, with still some contamination due to the presence of a small number of 30- and 60-minutes resolution timestamps. An internal source assessed that DMI uses a right labeled convention, meaning that the irradiance value stated at HH:10 is an average of the values between HH:01 and HH:10.

This point will be fundamental in the continuation of the project, in order to ensure a proper time alignment between the measurement and reanalysis datasets, as explained in Section 2.3 further on.

Instrumentation: descriptions and challenges

DMI measure global radiation from the six weather stations in Greenland using a 240-8101 Star pyranometer manufactured by Ph. Schenk, equipped with 240-8106 Protective Housing.

In 2024, DMI did modernized 3 stations with a new pyranometer, installing a SMP 10 manufactured by Kipp & Zonen in Ittoqqortoormiit (19/09/2024), Tasiilaq (01/10/2024) and Danmarkshavn (21/07/2024). New equipment is expected to be installed in the remaining three stations during summer 2025.

During winter, it is likely that the pyranometers are subject to icing phenomena. A pyranometer works with the Seebeck effect: a coated thermopile absorbs the radiation, heating up hence creating a temperature difference between the sensor surface and the body. When this involves metallic conductors or semiconductors, according to the Seebeck effect a voltage difference is generated. Such ΔV is proportional to the radiation.

It has been observed that, when covered by ice or frost, the voltage output of the pyranometer has a slight increase leading to an altered radiation measurement. [11] [12]

This effect is naturally particularly visible during the winter months, as shown in Figure 4: for the selected day, the effect is particularly visible for Ittorqortoormiit, Aasiaat and Narsarsuaq. The red line representing the measurements in Ittorqortoormiit never gets to 0 W/m^2 , but instead oscillates between 3 and 5 W/m^2 , while in Aasiaat the value is almost constantly equal to 1 W/m^2 and in Narsarsuaq it sporadically reaches small peaks of 1 and 2 W/m^2 .

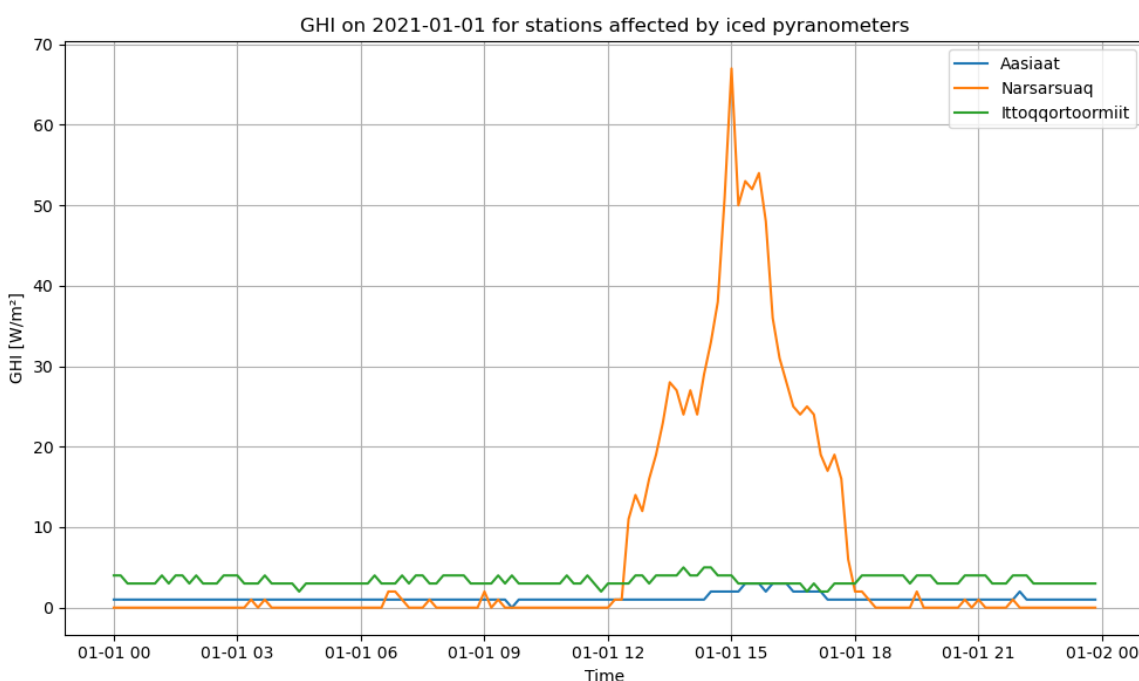


Figure 4: Iced pyranometer affects radiation measurements by slightly increasing the real value

2.1.2 Asiaq data

Asiaq do not provide freely online available data. From their website it was possible to understand that 12 out of their 39 Greenlandic weather stations measure solar irradiance and an attempt was made in order to obtain the data in question, which could have helped, on the side of the DMI one, to carry out a more thorough data validation process. However, despite numerous attempts to contact them via email asking for their ground measured data, there was never any response from the Greenlandic entity and a decision was made to continue the project without their support.

2.1.3 Quality control of the DMI data

After retrieval, the ground measurement data is subjected to a structured quality control process to evaluate the accuracy, completeness, and consistency of the raw DMI data. This process focuses on detecting and correcting anomalies, removing unreliable measurements, and preparing a validated dataset suitable for further analysis and comparison with other reference sources. [13]

2-D visualization

The first step is a two-dimensional visual inspection of the raw data which helps gaining a clear understanding of its consistency. In this visualization, the x-axis represents the days of the year, the y-axis represents the time of day, and the pixel color corresponds to the measurement value. One major advantage of this approach is that every data point is visible, allowing seasonal trends to be clearly observed, particularly with the help of the dashed red lines indicating sunrise and sunset. This method is especially useful for identifying time-dependent errors, such as time shifts or missing data.

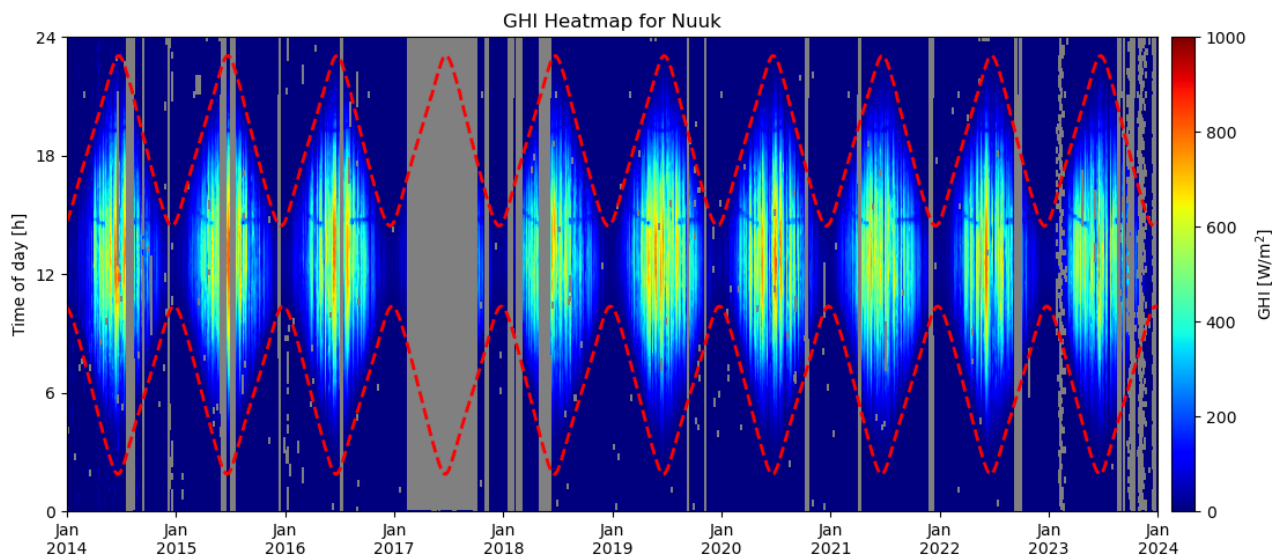


Figure 5: 2-D visualization of the raw data for Nuuk

Figure 5 shows the heatmap of the full dataset of the Nuuk station. The data coherence is confirmed by the fact that non-null irradiance values are included within the sunrise (on the bottom) and sunset (on the top) dashed lines, and the color scale varies accordingly to the lines' oscillation. Highest irradiance

is registered when the lines are the furthest away, namely in summer, when there's the biggest time distance between sunrise and sunset, while the winter data is close or equal to zero where the lines are closer.

Gray areas represent data unavailability. It is important to highlight that these plots represent the raw data starting from the first valid (not-NaN) irradiance value.

An interesting behavior can be observed for locations around or above the Arctic Circle, namely Aasiaat, Danmarkshavn, Ittoqqortoormiit and Tasiilaq. All these stations experience the midnight sun in the summer and the polar night in the winter, and, as can be seen for Ittoqqortoormiit in Figure 6 below, and for the remaining locations in Appendix C, the 2-D visualization is influenced.

The sunrise and sunset lines that become vertical during the summer months, the first vertical line being the last sunset after the beginning of the summer, and the second being the first sunset after the midnight sun. The distance between the two vertical lines is proportional to the distance between the station and the Arctic Circle: while for Tasiilaq, which is almost on the Circle, the two lines are almost overlaid, the plot for Danmarkshavn shows a remarkable distance between them, since the sun, at those latitudes, does not set from late April to mid August. [14]

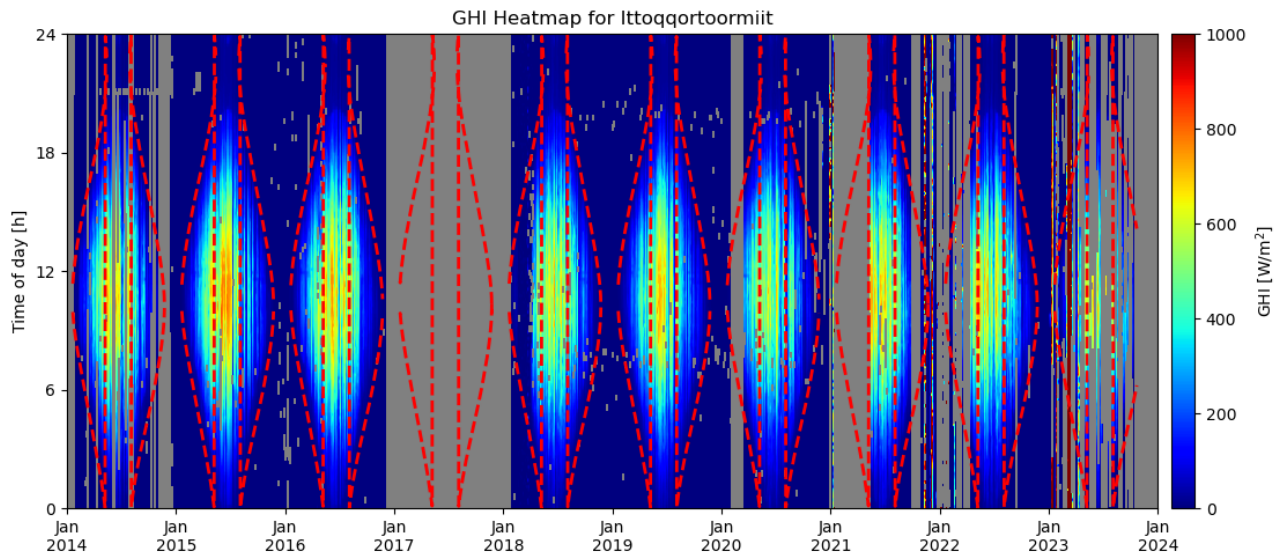


Figure 6: 2-D visualization of the raw data for Ittoqqortoormiit

Shading

The heatmap for Nuuk presented in Figure 7 alongside reveals recurrent anomalies (circled in black) occurring in the afternoon hours during the spring and autumn months throughout the observed time period. This consistent pattern initially suggested the presence of shading affecting the pyranometer. The hypothesis was substantiated through an inspection of the weather station's location on Google Maps: a pylon situated near the instrument appears to cast a shadow long enough to reach the pyranometer, thereby explaining the shading effect identified in the two-dimensional visualization. Figures 8 and 9 support this interpretation. In the satellite image, the yellow circle and arrow highlight the position of the pylon and the direction of its shadow, while the red marker indicates the pyranometer's location. In the on-site photograph, the instrument is circled in red, clearly showing its exposure to the pylon's shadow during certain times of the day.

Figures 10 and 11 below show the shading effect on the irradiance plots of two clear sky days in autumn 2017 and spring 2023 respectively. In both graphs, a sudden drop in irradiance is seen around 15:00, down to approximately 200 W/m^2 .

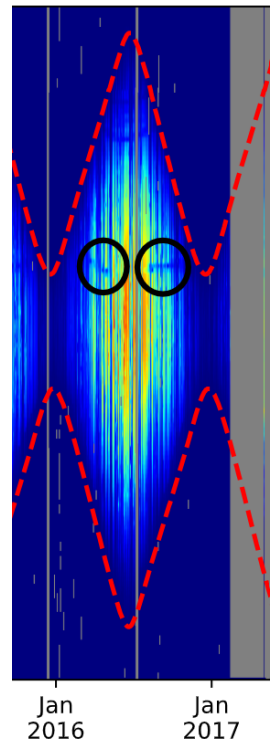


Figure 7: Anomalies in the Nuuk heatmap (2016)



Figure 8: Satellite view of the Nuuk station



Figure 9: On-site view of the Nuuk station

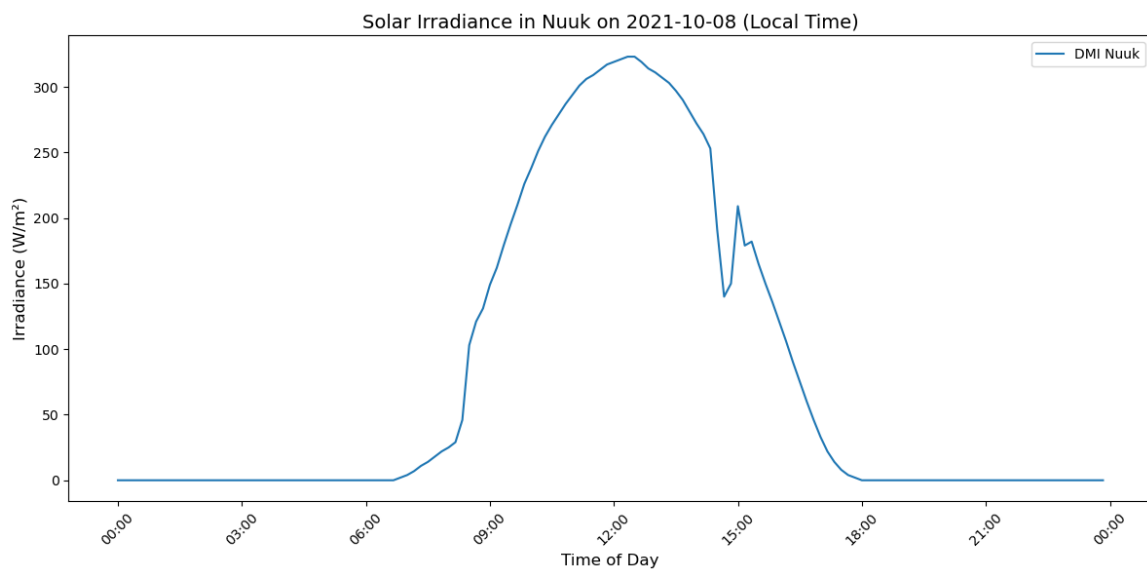


Figure 10: Effect of shading on an autumn day in Nuuk (2021)

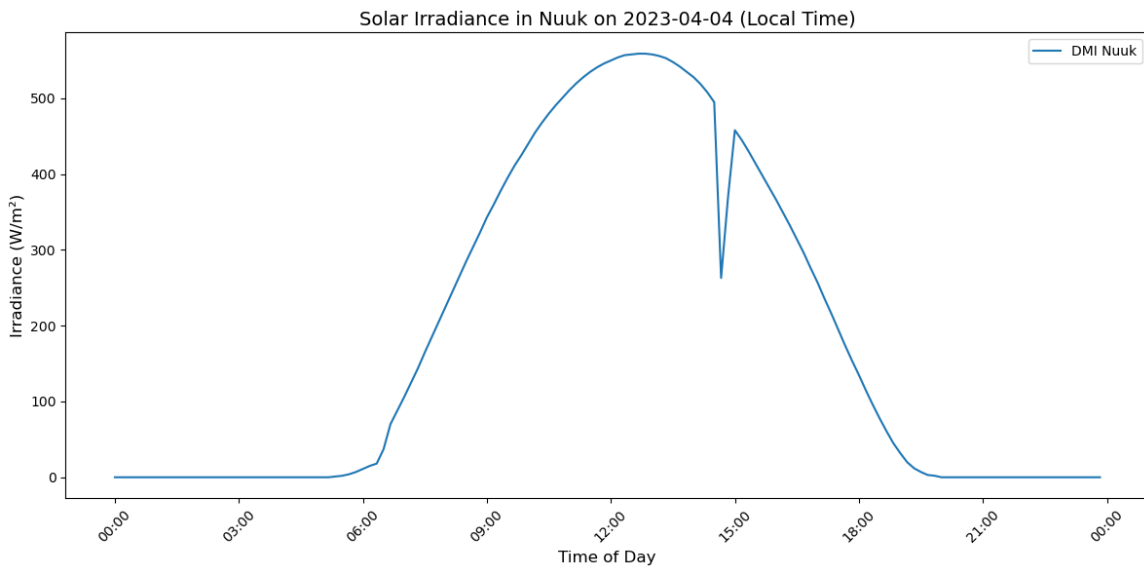


Figure 11: Effect of shading on a spring day in Nuuk (2023)

Data filtering

GHI vs time plots for single stations in single years confirm the imperfections already visible in the heatmap visualization, such as peaks exceeding realistic limits or instruments malfunctioning periods. This issue was solved using the following built-in python function of the pvanalytics library:

```
pvanalytics.quality.irradiance.check_irradiance_limits_qcrad()
```

The first step of the quality control process identifies and filters out invalid irradiance data using as inputs the initial GHI dataset, the solar zenith angle for the specific location and the extraterrestrial normal irradiance. It is important to highlight how this function is limited to deleting the abnormal values, but it does not substitute them with other values within realistic limits, nor fills preexisting gaps in the datasets.

Figure 12 shows the results of the quality control process for the GHI data for the Ittoqqortoormiit station in 2022. In the first months of the year, until April, there is a likely malfunctioning of the instrumentation, as the measurements are around 4000 W/m^2 for a prolonged time period. The two other peaks, at the beginning of May and at the end of August, are deleted as well.

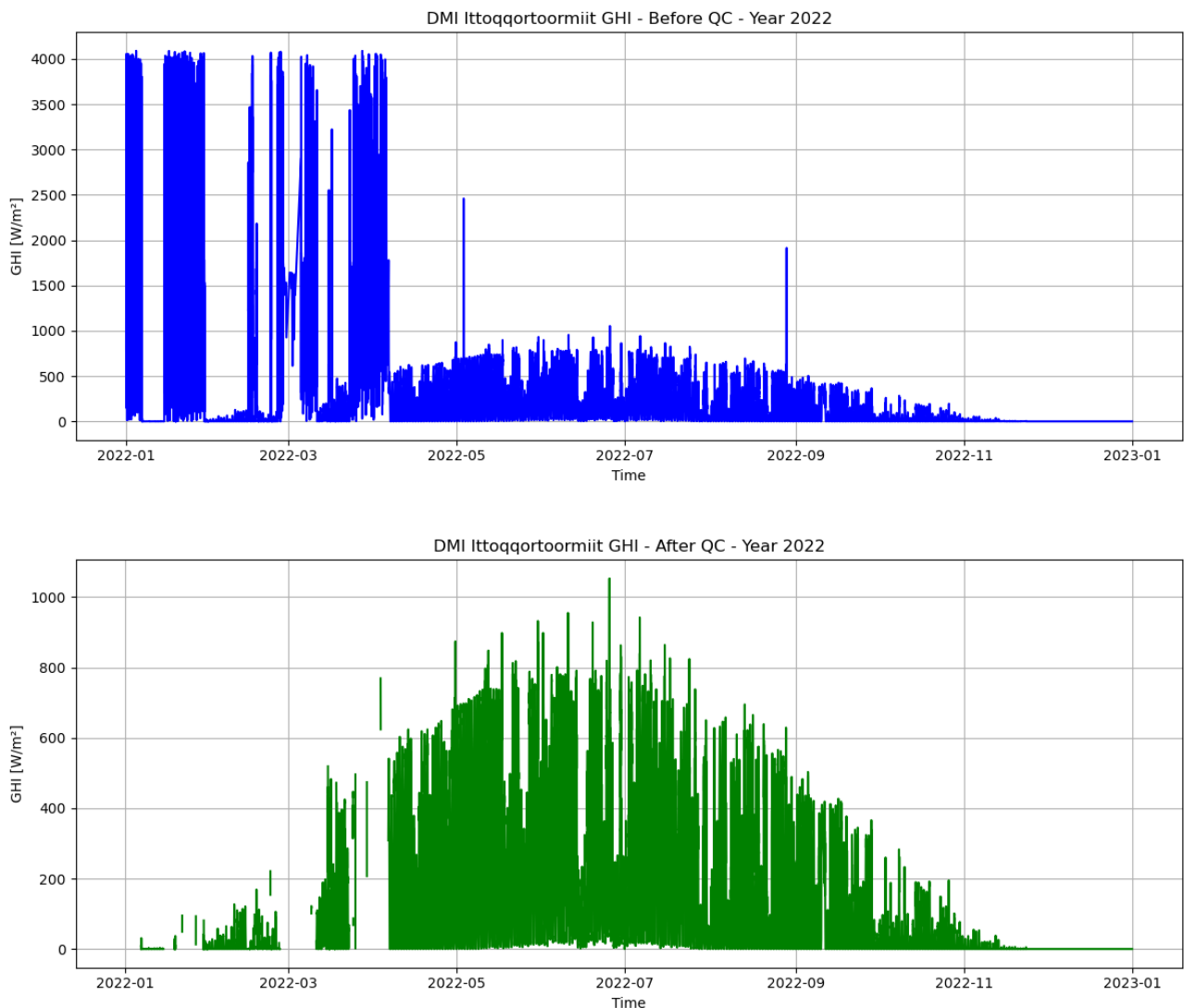


Figure 12: GHI dataset for 2022 in Ittoqqortoormiit before and after quality control

An additional step was incorporated into the data filtering process. The mentioned Python function assigns a binary flag (0 or 1) to each timestamp based on predefined thresholds determined by the site's geographic coordinates, indicating whether the associated irradiance values fall within acceptable bounds. Building on this, the new filtering criterion excludes entire days in which more than 50% of the timestamps are flagged as invalid, aiming to eliminate residual outlier data, such as the floating non-null values visible in the early months of Figure 12 or those illustrated in the plots of Figure 38 in the Appendix D, that remained after the initial filtering. However, the enhancement proved only partially effective, as not all anomalous values were removed.

A marginal improvement in the Root Mean Square Error (RMSE), that will be mentioned later in section 2.3, was observed, limited to the Narsarsuaq and Ittoqqortoormiit stations. The 50% threshold was deliberately not increased to prevent the loss of valid and potentially valuable data.

Another interesting behavior, observable for Ittoqqortoormiit and all the other locations interested by

the midnight sun phenomenon, is that during the summer months the radiation does not reach 0 W/m² creating a small empty area at the bottom of the graph.

Limits check

As the final step of the quality control process, the Physically Possible Limits (PPL) and Extremely Rare Limits (ERL) tests were applied to the GHI measurements, plotted against the solar zenith angle θ_z .

The PPL test assesses whether the measured irradiance values fall within physically feasible boundaries. The upper limits depend on the solar zenith angle, while the lower limit is set at - 4 W/m² to account for radiative cooling effects during nighttime, although under ideal conditions irradiance should not be negative.

The Extremely Rare Limits test applies more restrictive thresholds than the PPL test. Exceeding the ERL thresholds indicates measurements that are highly unlikely under typical atmospheric conditions.

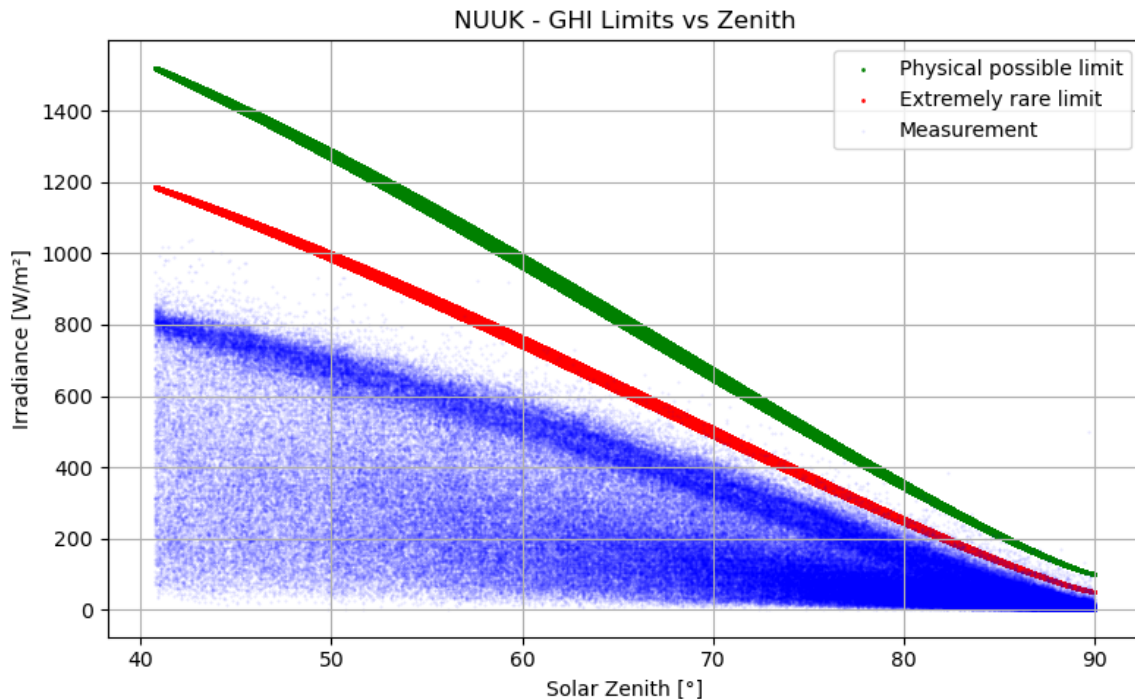


Figure 13: ERL and PPL thresholds check for Nuuk

In these representations, of which an example can be seen in Figure 13, green lines indicate the PPL thresholds and red lines indicate the ERL thresholds. The solar zenith upper limit was set at 90°, corresponding to a solar elevation of 0°, but for a more thorough check it can be extended to negative solar elevation values. A massive presence of blue dots in the $\theta_z > 90^\circ$ area would mean that an error occurred in the measurements at night or dusk. At the end of this process, the data was filtered deleting the values exceeding the ERL limits.

2.2 Modeled data

To validate the measurement data, a comparison with different modeled solar irradiance datasets was carried out.

This kind of data is usually divided into reanalysis and satellite datasets. Reanalysis datasets are derived from mathematical weather models combined with observational data, while satellite-derived irradiance time series are built on cloud identification based on satellite images. Reanalysis sets are preferred to satellite ones because of the latitude limit these are subject to: due to the view angle of geostationary satellites, they can provide information between latitudes of +60° and -60°, excluding Greenland from this range. ERA5 and NASA POWER are the two chosen reanalysis datasets, being easily and freely accessible online.

2.2.1 ERA5 data

ERA5 provides data for several parameters, and among those global radiation data for locations with latitudes lower than 75°N is available on the PVGIS (Photovoltaic Geographical Information System) website, provided by the Joint Research Center of the European Commission.

The downloadable solar radiation data is composed by plane of array direct irradiance, plane of array diffuse irradiance and plane of array ground-reflected irradiance. Selecting a 0° tilt angle on the website, it is possible to compute the GHI by adding up the 3 values. It is relevant to highlight that the ground reflected component is null, given an horizontal plan of array. PVGIS provides solar radiation data with an hourly frequency, from 2005 to 2023, in W/m². The timestamp format is HH:30, centered in the middle of the hour. Before moving on, it is important to highlight that, given the latitude restriction to 75°N imposed by PVGIS, ERA5 data is not available for the Danmarkshavn station, located further north than 76°.

2.2.2 NASA POWER data

NASA also provides a reanalysis dataset for meteorological and radiation parameters, NASA POWER (Prediction Of Worldwide Energy Resources), freely available on the power.larc.nasa.gov website for every latitude and longitude set, from 2001 to current days.

Unlike PVGIS ERA5, it is possible to access directly to GHI data without additional steps. NASA data is provided with an hourly resolution with the HH:00 timestamp format, and an internal source assessed that this dataset utilizes a left labeled convention, meaning that the irradiance value stated at HH:00 is an average of the values between HH:00 and HH:59.

It is again important to point out this dataset's and the ERA5 dataset's time formats (as also done in Section 2.2.1 above) in anticipation of the realignment among datasets that will be necessary during the data validation, described further in Section 2.3.

2.3 Data validation

After collecting both measurement and reanalysis datasets, a comparison must be conducted to evaluate their consistency and to determine whether they provide a reliable foundation for subsequent analyses.

Before starting with the validation process, it is important to highlight the decision to proceed with data included in the time interval between 01-01-2018 and 31-12-2023, for the following reasons:

- The lower limit was imposed because DMI data presents a 10-minutes resolution only starting from 2018. Before this date, data either had a hourly resolution or was partially missing, leading to the decision of using 2018 as the starting point, as mentioned in Section 2.1.1
- The higher limit is due to the fact that at the time of the research and writing, PVGIS only made ERA5 data available until the end of 2023, as explained in Section 2.2.1.

Moreover, some years were excluded from the benchmark for the different stations, in order to avoid using bad quality data, because of missing parts or bad time resolution of the DMI dataset. Table 2 describes the chosen years for all the different stations.

Table 2: Years excluded from the 01-01-2018 to 31-12-2023 interval for the different stations

Station name	Excluded years
Nuuk	None
Aasiaat	None
Narsarsuaq	2018
Ittoqqortoormiit	2021, 2023
Tasiilaq	2018
Danmarkshavn	None

The previous sections outlined the varying timestamp conventions used by the three data providers, making it essential to appropriately shift the datasets to align them and account for these differences.

DMI data is first given homogeneous time steps by using the `.asfreq('10min')` python function, and is subsequently sampled as right labeled and right closed and resampled as hourly, making an average of the ten minutes data. To adapt to the DMI reference, the other datasets are aligned and also made right labeled: ERA5 is shifted forward by 30 minutes, while NASA POWER forward by 60 minutes.

After the alignment, the datasets were compared using a scatterplot for a visual approach, accompanied by an RMSE calculation for a quantitative evaluation. The results are reported in Figure 14 for the Nuuk station (see Appendix E for all the plots) and in Table 3.

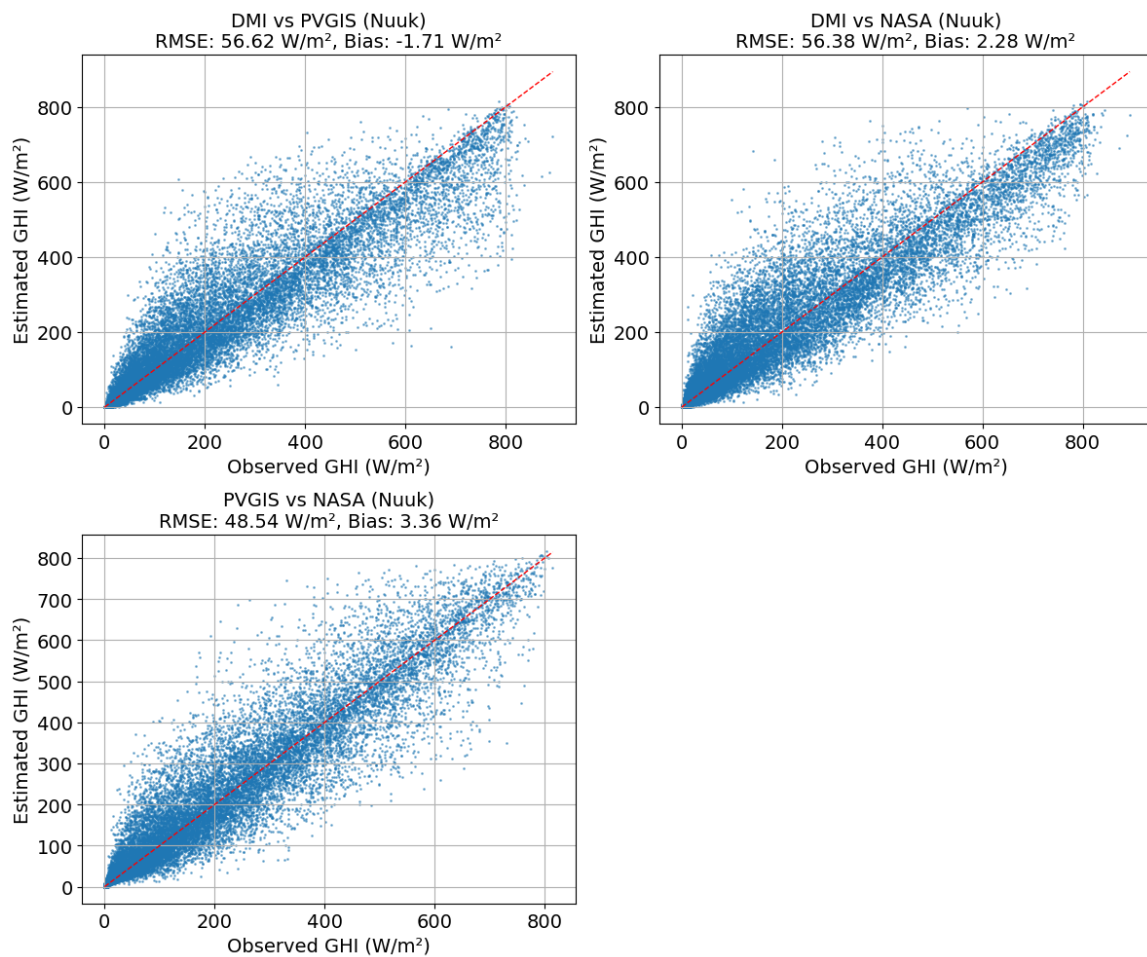


Figure 14: Scatter plots for Nuuk

Table 3: Resulting RMSE [W/m²] values after data validation.

	DMI vs ERA5	DMI vs NASA	ERA5 vs NASA
Nuuk	56.62	56.38	48.54
Aasiaat	53.22	45.91	44.33
Narsarsuaq	67.78	96.87	93.43
Ittoqqortoormiit	57.49	55.48	38.31
Tasiilaq	56.68	64.18	53.56
Danmarkshavn	-	41.40	-

Table 3 revealed notably higher RMSE values for the Narsarsuaq station when the NASA dataset was included, warranting a more in-depth investigation. Examination of the corresponding scatter plots suggests that the NASA dataset tends to systematically overestimate both DMI and ERA5 values in the medium to low irradiance range, approximately between 0 and 400 W/m². To substantiate this observation, time series plots for selected spring and summer months were generated and visually compared across the three datasets.

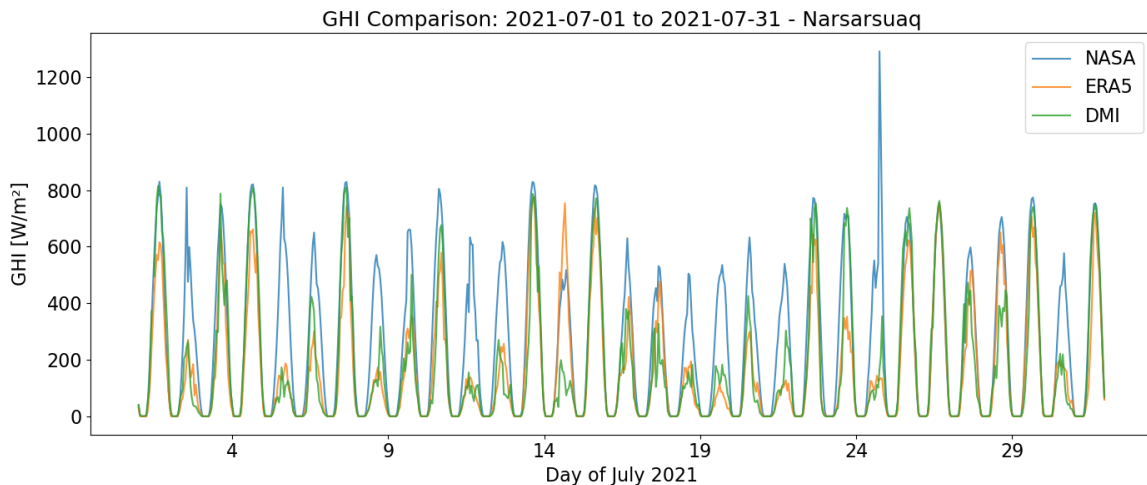


Figure 15: Comparison of the three datasets in Narsarsuaq for July 2021

As shown in Figure 15, the NASA data (blue line) consistently reports higher irradiance values compared to ERA5 (yellow) and DMI (green), particularly for GHI values below 400 W/m^2 . This trend is evident across multiple days in the month of July 2021. Additionally, NASA data exhibits extreme peaks, such as the one on July 24, where the GHI exceeds 1200 W/m^2 . This value is well above the realistic physical limit of 1000 W/m^2 under clear-sky conditions and is indicative of the frequent outliers observed in NASA data for this location (see Figure 42, for example).

In parallel to the RMSE, it is also useful to calculate the bias, to find whether the model systematically overestimates or underestimates the observed values, which is essential for assessing and enhancing the reanalysis datasets' accuracy and reliability. Table 4 reports the results of this analysis.

Table 4: Resulting bias [W/m^2] values after data validation.

	DMI vs ERA5	DMI vs NASA	ERA5 vs NASA
Nuuk	-1.71	2.28	3.36
Aasiaat	2.25	-6.90	-9.15
Narsarsuaq	-6.72	30.85	37.60
Ittoqqortoormiit	-5.45	-4.64	0.25
Tasiilaq	-6.53	-17.17	-11.57
Danmarkshavn	-	-6.82	-

The same analytical procedure was repeated for other spring and summer months across the full range of years studied, and the results were consistent with the observations reported above. A further analysis was conducted using the average values and the standard deviations for RMSEs and absolute biases of DMI vs ERA5 and DMI vs NASA, to have a more concise and meaningful overview, and its results are reported in Table 5 below. Absolute biases are preferred over relative biases to avoid the cancellation of positive and negative values, which can hide the actual size of the differences when calculating averages and standard deviations.

Table 5: Comparison of DMI data against ERA5 and NASA: RMSE and absolute bias statistics.
[W/m²]

DMI vs ERA5			DMI vs NASA		
	RMSE	Absolute Bias		RMSE	Absolute Bias
Average	58.36	4.53		60.04	11.45
StDev	4.93	2.13		18.05	9.85

Table 6: Comparison of DMI data against ERA5 and NASA: RMSE and bias statistics. [W/m²]

DMI vs ERA5			DMI vs NASA		
	RMSE	Bias		RMSE	Bias
Average	58.36	-3.63		60.04	-0.40
StDev	4.93	3.45		18.05	15.09

Table 6 was added in order to highlight the distorting effect that the adoption of a non-absolute bias would have had on the statistical analysis, in particular for the average value. It increases using the absolute bias, because the lowering effect due to the cancellation of minus and plus signs is avoided and the result is then a more realistic value.

The standard deviation is also affected by the choice of an absolute bias usage, but not as heavily as the average.

Looking at the values reported above, it can be observed that the average values of the two comparisons are not distant, with the average RMSE being slightly better for ERA5 which has however a marginally worse average bias. The standard deviation value is instead more indicative: the NASA dataset's RMSE and bias are subject to a much higher variability, which also gives a lower relevance to the low average values described above. Based on these results, ERA5 was selected for further use due to its greater consistency across stations. While the average metrics of the two datasets are comparable, the significantly lower variability in both RMSE and bias for ERA5 indicates more stable and reliable performance, which is crucial for accurate and reproducible modeling.

3 PV energy potential

The next step of the project is to use the chosen reanalysis dataset to model a photovoltaic plant to generate electric energy for Greenlandic settlements in an alternative way to fossil fuels. The plants will consist of fixed ground-mounted bifacial solar panels and roof-mounted monofacial modules.

This analysis was planned to be undertaken for the settlements of Qeqertarsuatsiaat and Ilimanaq, chosen for the reason that Nukissiorfít provided consumption data for 2023 for those two locations only, courtesy of Esben Lundø Madsen. [15] The consumption numbers will be used in the analysis of Chapter 4 to study the compatibility of the production of renewable energy and the local demand.

Qeqertarsuatsiaat is a small settlement in southwestern Greenland with a population of approximately 170 inhabitants. It is situated around 130 km south of Nuuk and over 300 km north of Qaqortoq, where the Qorlortorsuaq hydropower plant is located. Given the significant distances from the nearest hydropower facilities, it is reasonable to assume that Qeqertarsuatsiaat relies primarily on diesel-generated electricity. In the absence of publicly available data confirming the local energy mix, this assumption serves as a plausible basis for analysis.

Ilimanaq is a small settlement located on the western coast of Greenland, with a recorded population of 53 inhabitants in 2020. It is situated approximately 15 km south of the Paakitsoq-IIulissat hydropower plan in Ilulissat. The two locations are separated by Disko Bugt (Disko Bay), a bay known for its intense glaciological activity, evidenced by the frequent presence of icebergs detached from the Sermeq Kujalleq (Jakobshavn Glacier). This geographical barrier is a substantial challenge to infrastructure connectivity, particularly for energy transmission. Consequently, in line with the assumptions made for Qeqertarsuatsiaat, it is presumed that Ilimanaq relies exclusively on diesel-generated electricity in the absence of other accessible energy sources.

The locations of the settlements can be seen in Figure 44 in Appendix F, and compared with those of the hydropower plants in the previously mentioned Figure 32 in Appendix A.

3.1 Modeling a PV plant

The first required action was retrieving the ERA5 GHI data for Qeqertarsuatsiaat and Ilimanaq from PVGIS, as explained in Section 2.2.1 above. Since both towns are located below 75°N, the adoption of this reanalysis dataset did not constitute a problem as they're both within the website's limitations. Given the availability of consumption data for 2023 only, ERA5 data was retrieved just for that year.

As explained previously, PVGIS provides irradiance data broken down into plane of array direct irradiance, plane of array diffuse irradiance and plane of array ground-reflected irradiance, making it possible to calculate GHI when a 0° surface tilt angle is selected on the website.

The `pvlb.irradiance.get_total_irradiance` function in Python can be used to compute the total plane-of-array irradiance incident on mono-facial panels. This function requires several inputs, including the surface tilt, which is the angle between the panel surface and the horizontal plane, and the surface azimuth, which refers to the cardinal direction the panel is facing. The azimuth angle is defined as explained in Section 3.1. Another required input is the solar zenith, which is the complementary angle to the solar elevation and depends only on the geographical coordinates of the panel.

The function also requires DNI, DHI, GHI (introduced in Section 2) and the extraterrestrial direct normal irradiance, the solar radiation received on a surface normal to the sun's rays at the top of Earth's atmosphere: all these quantities should be expressed in W/m².

The albedo factor must be specified as well: it is the ratio of reflected to incoming solar radiation on a surface, and is a unitless value between 0 and 1, depending on the characteristics of the soil where the panel is installed. Finally, the sky diffuse irradiance model must be defined to estimate the amount of solar radiation reaching the Earth's surface in the absence of cloud cover. The choices of albedo factor and clear sky model are described in Sections 3.1.1 and 3.1.3 below.

The process described above to obtain the global plane-of-array irradiance is only valid for mono-facial panels, and will be used, in the next step, just for performance simulations of roof-mounted systems. For bifacial panels another Python function was used, `pvlib.bifacial.infinite_sheds.get_irradiance`, which requires the same inputs as above plus some additions: the Ground Coverage Ratio (GCR), which is the ratio of row slant length to row spacing; the height, describing the elevation of the center point of the row of panels above the ground; the pitch, which is the distance between two rows of panels; finally, the bifaciality fatcor, whose choice is explained in Section 3.1.3.

The optimal GCR value for a PV plant varies depending on the type of plant in question (mono-facial/bifacial and tracking/fixed tilt/vertical) and on the latitude it is built at. From Figure 16 it is possible to extrapolate that the ideal GCR for a bifacial plant, built at the latitude of Ililamaq (69.079° N) is between 0.15 and 0.2 for both bifacial fixed-tilt and bifacial vertical panels. An average value of 0.17 is assumed for both categories. [16]

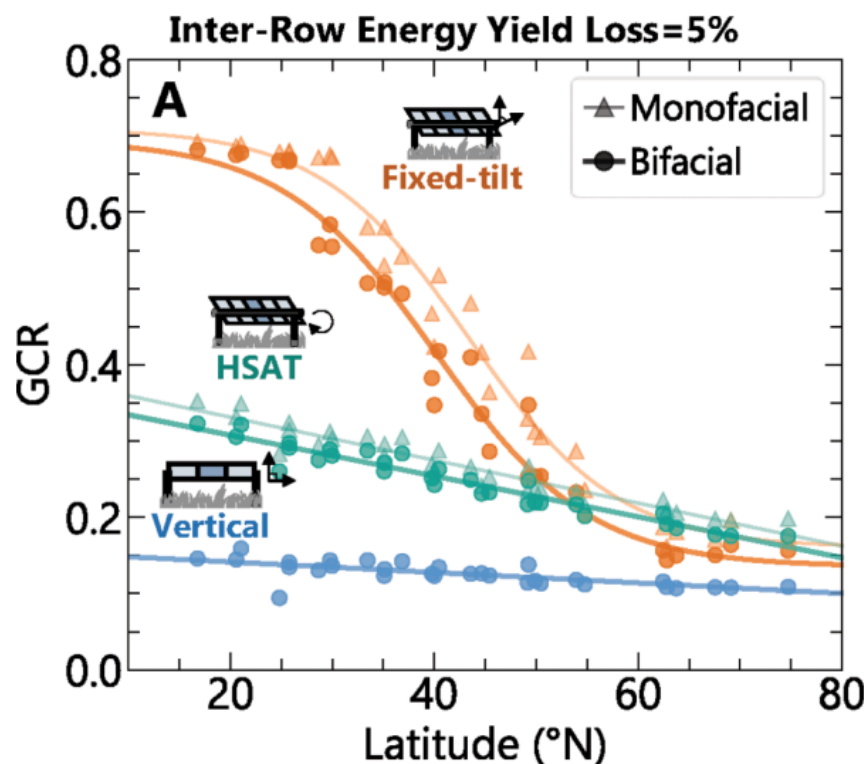


Figure 16: Optimal GCR values depending on plant location and typology.[16]

Height (H) and pitch (P) values were calculated starting from the good practice of mounting non-tracking solar arrays at a narrow distance from the soil, since there is no need for room for rotation of the panels: hence, a ground clearance (GC) of 50 cm was chosen. Given that modern modules have a length (L) of around 2 m, height can be computed with a simple trigonometric operation:

$$H = GC + \frac{L}{2} \cdot \sin(\beta) \quad (2)$$

The result is that, changing the input tilt angle β , H will vary from simulation to simulation.

About the pitch (P), it is calculated according to the formula:

$$P = \frac{L}{GCR} \quad (3)$$

This means that, with the adopted values of L=2 m and GCR=0.17, P has a constant value of 11.7 m.

3.1.1 Albedo

Albedo factor, as mentioned in Section 3.1, is defined as the ratio between reflected and incoming solar radiation on a surface, and depends on the characteristics of the soil. When it comes to PV applications and modeling, it is then important to characterize the type of soil the panels are mounted on, as it defines the albedo which consequently determines the amount of ground reflected radiation available for energy conversion.

It is particularly important for the modeling of a bifacial panel because for this types of systems ground-reflected radiation typically accounts for around 10% of the effective irradiance received by bifacial photovoltaic systems globally. [17]

Given their white color, snow and ice have a high reflectance value and hence high albedo factors, which get progressively worse as they melt or become dirty. Table 7 shows the variation of albedo factors according to snow and ice types. [18]

Table 7: Typical albedo values for different snow and ice types [18]

Snow/Ice Type	Albedo Range
Dry snow	0.80–0.97
Melting snow	0.66–0.88
Firn	0.43–0.69
Clean ice	0.34–0.51
Slightly dirty ice	0.26–0.33
Dirty ice	0.15–0.25
Debris-covered ice	0.10–0.15

Qeqertarsuatsiaat and Ililanaq are coastal towns, meaning their and their surroundings' territory is partially or fully covered by snow between September and May every year, while bare soil, which has an estimated albedo value of 0.2, emerges during the summer months. This discontinuity of soil type

makes choosing one single albedo factor for the whole year an unacceptable approximation: it is then necessary to estimate plausible values for the whole year.

From online databases for Nuuk (taken as a reference for Qeqertarsuatsiaat) [19] and Ilulissat (taken as a reference for Ilimanaq) [20], the monthly average cumulated snowfall were found, and are reported in Table 8.

Table 8: Monthly Snowfall in Nuuk and Ilulissat (in mm)

Location	Jan	Feb	Mar	Apr	May	Jun	Jul	Aug	Sep	Oct	Nov	Dec
Nuuk	222.7	193.6	192.0	163.4	39.5	1.7	0.0	0.0	4.7	60.4	191.6	247.3
Ilulissat	59.1	78.6	77.4	96.9	51.1	6.3	0.2	0.2	14.9	83.8	132.4	87.6

It is then possible to conclude that the soil in both is snow-free in July and August only, covered by just a few millimeters in June and September and by a thick layer of fresh snow in all the other months. None of the Greenlandic settlements are part of the ice sheet: it is then decided to adopt dry snow albedo from October to April, melting snow albedo in May, June and September, bare soil albedo for July and August, using average values extracted from the intervals reported in Table 7. The chosen values are reported in Table 9 below.

Table 9: Chosen albedo factor for each month

Location	Jan	Feb	Mar	Apr	May	Jun	Jul	Aug	Sep	Oct	Nov	Dec
Both	0.89	0.89	0.89	0.89	0.77	0.77	0.2	0.2	0.77	0.89	0.89	0.89

3.1.2 Clear sky model

The `pvlb.bifacial.infinite_sheds.get_irradiance` function uses the isotropic clear sky model as a default, which is based on the hypothesis that all diffuse irradiance is uniformly diffused. The reality is that irradiance is actually anisotropic: diffuse irradiance mostly comes from the circumsolar region, the area of the closely surrounding the sun disk where scattered solar radiation is concentrated due to forward scattering by atmospheric particles, instead of coming uniformly from all around the sky dome. [21] Many anisotropic models exist, but the function only accepts the Hay and Davies model as an alternative to the isotropic.

3.1.3 Bifaciality

The bifaciality factor indicates the performance of the back of a panel compared to the front of the same: a factor of 1 means the back of the solar panel is equally as efficient as its front. Since a specific model of solar panel was not chosen, an average bifaciality factor of 0.8 was selected to proceed with the simulation.

3.2 Electricity consumption data description

The consumption data [15] is provided into two Excel files, in kWh and with an hourly resolution. The Qeqertarsuatsiaat dataset includes 5952 timestamps, out of the 8760 yearly hours of a non-leap year as 2023, while the Ilimanaq datasets is composed by 8395 single data points. This last value was

particularly noticeable because it is exactly 365 timestamps away from the total of 8760: a further observation of the dataset revealed that every timestamp relative to midnight for all the days of the year is missing, with the time switching directly from 23:00 of the n-th day to 01:00 of the following. To remedy this problem, a linear interpolation was made; by doing so, the Ilimanaq dataset is completed.

On the other hand, in the Qeqertarsuatsiaat dataset there are 92 days fully missing, as reported in Table 10

Table 10: Missing days per month, Qeqertarsuatsiaat dataset

Month	Missing Days
2023-01	4
2023-03	4
2023-04	18
2023-05	7
2023-06	3
2023-08	19
2023-09	13
2023-10	15
2023-11	7
2023-12	2

To solve the problem created by such frequent gaps, for each month an average daily consumption was calculated, and the resulting value was then multiplied by the number of days of the respective month. By doing so, a full averaged dataset was obtained for this settlement as well. Table 11 reports the obtained consumption values for the two locations. The corresponding bar plots are reported in Appendix G.

Table 11: Monthly energy consumption comparison for 2023 (in MWh)

Month	Ilimanaq (MWh)	Qeqertarsuatsiaat (MWh)
January	54.8	84.0
February	48.3	80.0
March	50.8	88.3
April	44.4	81.5
May	47.5	70.6
June	64.0	76.1
July	53.1	65.0
August	50.4	73.7
September	52.7	74.3
October	38.7	83.7
November	39.1	77.7
December	47.9	82.7
Total	591.6	937.6

Because of the many gaps present for Qeqertarsuatsiaat, the dataset was considered unreliable even after the undertaken averaging activity. Ilimanaq will then be the only location to be considered in the continuation of the project for solar energy production simulations purposes.

3.3 Simulate PV production

The final step, following the structure outlined in the previous sections, is to run a series of simulations assessing the photovoltaic production of a power plant in Ilimanaq with varying capacities, ranging from 100 kW to 500 kW, with a 50 kW step from time to time. This approach aims to replicate the development of similar-sized installations in the region and to evaluate at which point increasing the system size becomes inefficient. Beyond this threshold, additional capacity leads to overproduction and, consequently, increased energy curtailment. For brevity purposes, the results in the tables in each subsection are only reported for capacities multiple of 100 kW.

Simulations are deployed for monofacial (roof mounted) and bifacial (ground mounted) systems, with tilts of 60° and 90°, for ground mounted systems, and 40° for roof-mounted systems, and azimuth angles of 90° (East-facing), 180° (South-facing), and 270° (West-facing).

The choice of the 60° tilt is given by the rule of thumb of selecting a tilt some degrees lower than the latitude of the chosen location (69° for Ilimanaq), and values around 60° were having the best outputs in the first tries, and the number was selected in order to have a round figure. Vertical panels are widely adopted in the Arctic regions because of their ability to catch more radiation from all the directions even with low solar altitudes, while, for purposes of realism, the tilt of 40° was adopted as a reference value for pitched roofs in Greenland, thanks to the input kindly provided by Tove Lading via personal communication.

Once the PV production is obtained at the end of the simulation, it is compared with the consumption data described in Section 3.2 to compute the displaced energy, meaning the amount of energy previously obtained via diesel combustion that is substituted by renewables, solar in this study case. Assuming the constancy of consumption data, it is an interesting to observe the trend displaced energy undertakes in response to a hypothetical growth of PV production: the expectation is that after an initial linear growth of the total yearly displaced energy, the curve will start flattening when the high capacity becomes unnecessary to the settlement needs, resulting in overproduction and a subsequent energy curtailment. For this purpose, the PV production results are multiplied by factors of 2, 3, 4 and 5, to simulate the construction of other similar plants in the area and to study after how long the growth becomes inefficient,

Moreover, the share of yearly PV production over total yearly energy consumption is also computed, in order to investigate the impact that the adoption of this alternative source brings.

In the next chapter, from Section 4, are reported the results of the analysis for the different scenarios.

3.3.1 Snow coverage of the PV panels

One final factor to be considered is the accumulation of snow and ice on the surface of photovoltaic panels, which can reduce solar irradiance and, consequently, electricity generation. Studies have investigated this effect, estimating annual generation losses across different climatic conditions, typically categorized as severe, moderate, or mild based on ambient temperatures and annual snowfall [22].

Although winter temperatures in Ililanaq are extreme, the location experiences relatively mild snowfall. Based on the data reported in Table 8 for Ilulissat — situated approximately 15 km from Ililanaq, as mentioned in the introduction to Section 3 — the average annual snowfall is approximately 70 cm. This places Ililanaq within the “mild snowfall” classification.

According to the findings in [22], snow-related losses for PV systems with a tilt angle of 40° to 45° in moderate snowy climates range from 0.9% to 1.7% of the annual energy yield. These losses decrease further for steeper panel tilts, with losses dropping below 1% for 60° tilts and reaching as low as 0.3% for vertical installations under comparable conditions.

Such losses are concentrated in the winter months, during which solar production at high latitudes is already minimal or negligible. Consequently, the impact of snow accumulation on annual PV performance is marginal. For this reason, snow-related energy losses have been considered negligible in the subsequent simulation steps.

4 Results

Simulations were run following the structure described in Section 3.3, and below are reported the results, scenario by scenario, beginning from tilted bifacial systems, followed by vertical bifacial systems, to simulate ground-mounted PV plants, and finally tilted monofacial systems, that reproduce roof-mounted panels.

4.1 Bifacial panels, tilted by 60°

The first reported results are those relative to a PV plant of ground-mounted bifacial solar panels, tilted by 60° with respect to the horizontal.

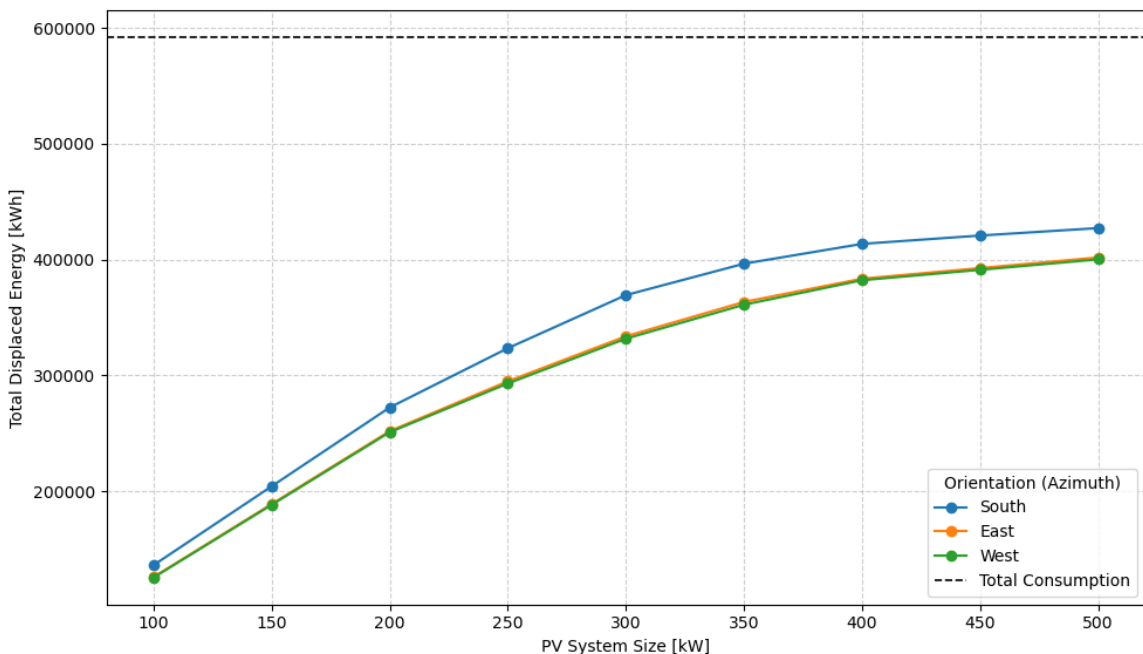


Figure 17: Growth trend of the displaced energy in Ililamaq with increasing PV capacity.
Bifacial panels, tilt = 60°

Table 12: Annual displaced energy [MWh] for different system sizes and orientations.

Scenario	100 kW	200 kW	300 kW	400 kW	500 kW
South	136.1	272.3	369.3	413.5	427.1
East	125.9	251.9	333.7	383.4	401.8
West	125.5	250.9	331.6	382.1	400.1

Looking at Figure 17 and Table 12, it is possible to observe a decreasing growth pace of the total displaced energy due to the adoption of a 60° tilted PV system when the size of it increases, for all the tested orientations, and Figure 17 also reports the total yearly energy consumption of Ililamaq, that amounts to 591.6 MWh, as a dashed black horizontal line.

For all the tested azimuths, the displaced energy doubles with the initial doubling of the

photovoltaic capacity from 100 to 200 kW, and the corresponding 0% of curtailed energy percentage testify that there is no waste of solar energy.

The trend changes when the capacity grows to 300 kW, and the displaced energy just goes from a 100% growth of the previous step, to a displaced energy growth of around 35% with a 50% increase in capacity.

When the PV capacity grows further, from 300 to 400 and subsequently 500 kW, the curve flattens due to a very small increased of total displaced energy.

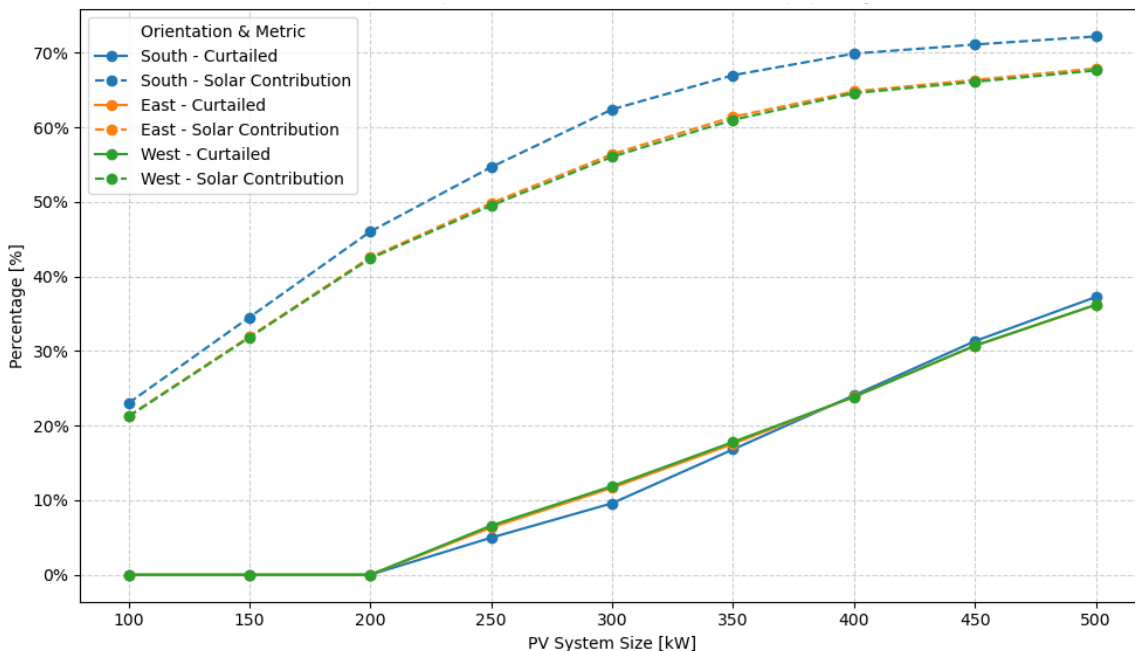


Figure 18: Growth trend of curtailed energy and solar contribution in Ilimanaq with increasing PV capacity.

Bifacial panels, tilt = 60°

Table 13: Curtailed Energy Percentage [%] by System Size [kW] and Orientation
Bifacial, 60° tilt

Scenario	100 kW	200 kW	300 kW	400 kW	500 kW
South	0.0	0.0	9.6	24.1	37.3
East	0.0	0.0	11.7	23.9	36.2
West	0.0	0.0	11.9	23.9	36.2

Figure 18 and Table 13 instead report the growth of the percentage of the generated solar energy that gets curtailed, meaning not consumed by the Ilimanaq community - and consequently wasted given the lack of planned storage technologies in this project - when the PV capacity grows; alongside it, there is the solar contribution percentage, defined as the ratio between non-curtailed energy and total consumption, also growing with the trend that's been already detected for displaced energy in Figure 17. For this case, curtailment starts when the solar share is approximately 46% for South-facing modules, and approximately 42% for the other two azimuth angles.

In this scenario, there's no curtailed energy for the 100 and 200 kW cases, meaning that all the PV-produced energy is consumed. When the capacity reaches 300 kW, the percentage starts growing and it is interesting to highlight how it is lower when the panels face South, despite this being the orientation resulting into the highest production, as shown in Appendix H.1.

It could be hypothesized that bigger energy production leads to greater waste, but the distribution of the produced energy throughout the months plays a crucial role in this calculation. Figures 19, 20 and 21 below provide a better understanding of the results.

When the azimuth is 180° (for reference, see Figure 19 and Figure 47), i.e the panels are facing South, the overall production is the highest but less energy is curtailed because an important production growth is visible in low-radiation months like March, September and October, and such an increase in production does not overcome the consumption value and hence does not result in any curtailment. Such a growth in those months balances the curtailed energy of the months between April and June, when the consumption is overtaken by the production for all three orientations.

When the PV capacity increases again, to 400 and 500 kW, this effect is lost due to the bigger gaps created by a much higher production, and all the three orientations have similar percentages.

Looking at the dashed line, representing the solar contribution. This indicator is very strictly linked to the energy curtailment: it is clear how the growth rate is linear at the beginning of the simulation, when the curtailed percentage is null, for low capacities, and starts slowing down as soon as energy starts being unused. This is because non-curtailed energy is utilized in the calculations of solar contribution, being divided by the total consumption, it is naturally consequential that a rising waste of solar energy gives a growth in production with decreasing pace.

In this case, the solar contribution flattens around a value of 70% and reaching higher values would require a massive effort in terms of extension of the capacity, that would however bring low benefits. This upper limit allocates so distant from the 100% maximum value because of the impossibility of filling the consumption/production gap in winter times, when the solar radiation is almost constantly equal to zero, hence creating an insurmountable obstacle to the achievement of higher values.

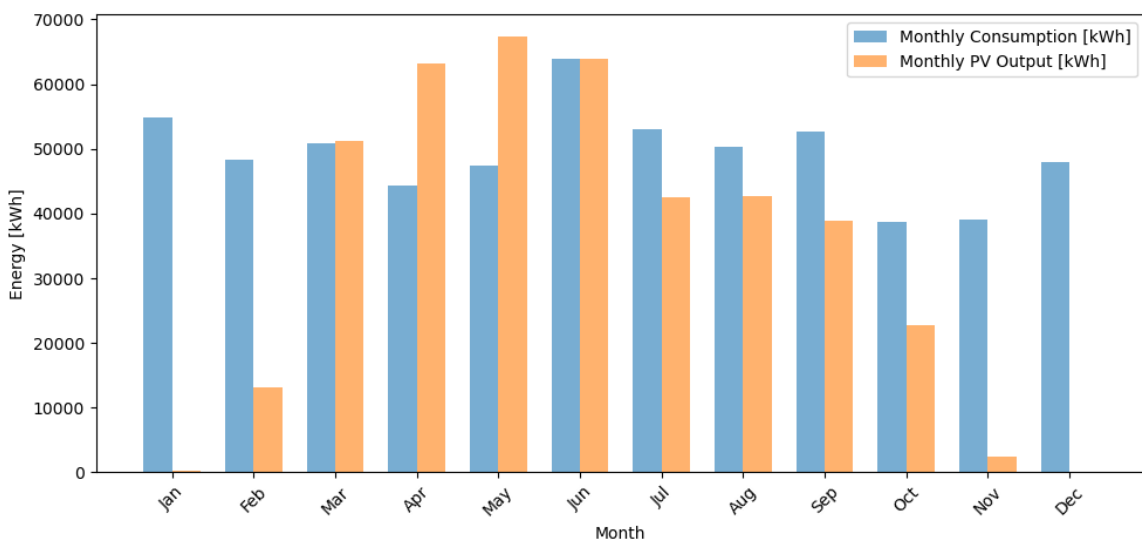


Figure 19: Monthly comparison of PV energy production and the Ililamaq energy consumption.
Bifacial panels, tilt = 60°, azimuth = 180°

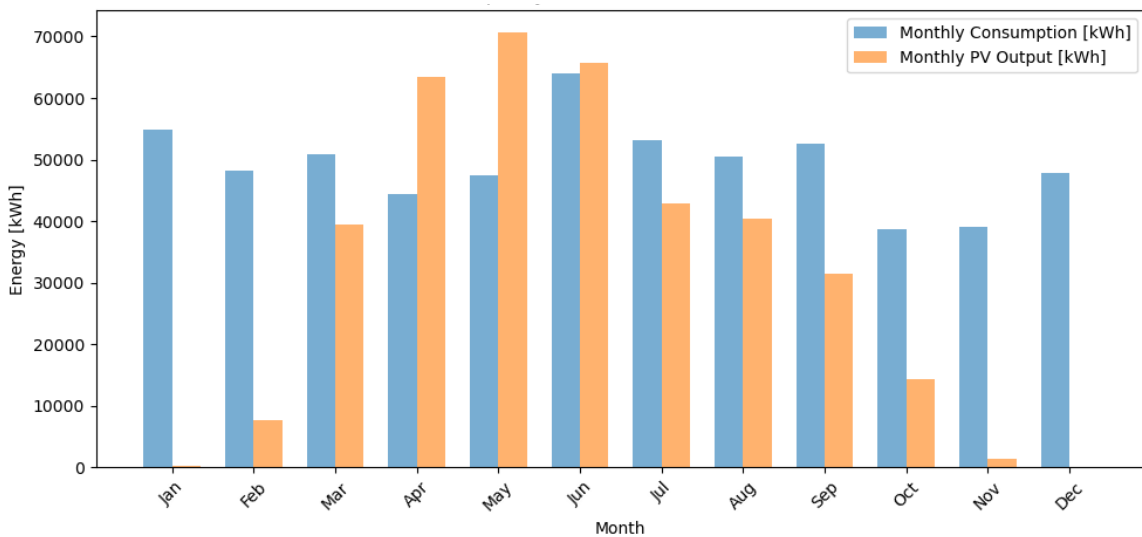


Figure 20: Monthly comparison of PV energy production and the Ililamaq energy consumption.
Bifacial panels, tilt = 60°, azimuth = 90°

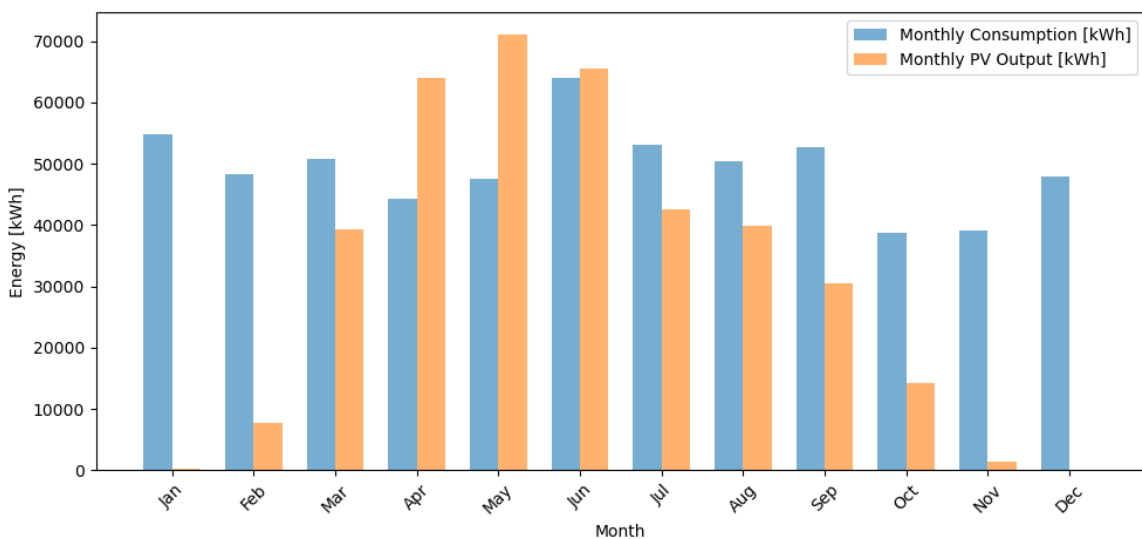


Figure 21: Monthly comparison of PV energy production and the Ilimanaq energy consumption.
Bifacial panels, tilt = 60° , azimuth = 270°

Appendix H.2 reports an analysis for 45° tilted bifacial panels.

4.2 Vertical bifacial panels

The following, and last, analyzed set of bifacial panels are the vertical.

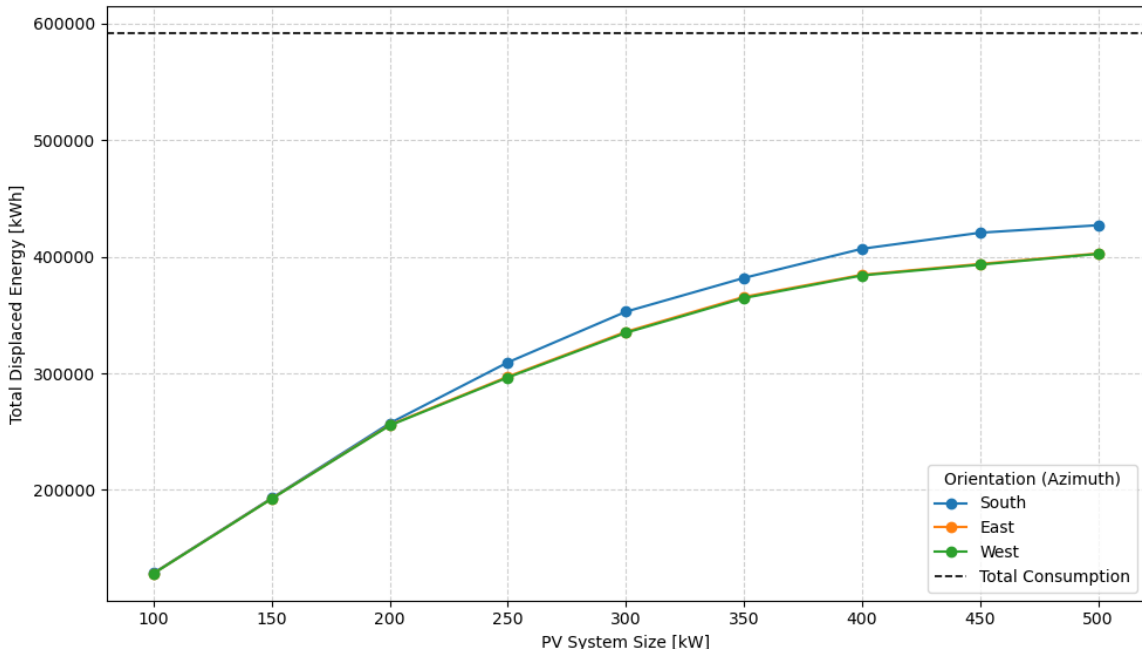


Figure 22: Growth trend of the displaced energy in Ilimanaq with increasing PV capacity.
Bifacial panels, vertical

Table 14: Annual displaced energy [MWh] for different system sizes and orientations.
Bifacial panels, vertical

Scenario	100 kW	200 kW	300 kW	400 kW	500 kW
South	128.6	257.1	352.9	406.9	427.1
East	128.3	255.6	335.6	384.5	402.9
West	128.2	255.2	334.8	384.0	402.5

The displaced energy values of a system of vertically ground-mounted panels have the same trend of the cases above. If the panels are oriented towards South, the resulting values are slightly lower than the corresponding ones of the previous analyses for capacities up to 300 kW, when the overproduction starts leveling the different scenarios.

Vertical West- and East-facing systems have, on the other hand, higher values than the ones of 45° and 60° from a 4-5% increase in the low capacity simulations to 1% in the higher ones. It is also interesting to point that, with the adoption of vertical panels, the gap between the displaced energy of South and East/West facing panels is reduced: from a 8 and 9% average difference for 60° and 45° tilts respectively, this gap shrinks to an average 3% difference, and is even lower for the low capacity options. The reason this happens is to be found in Figures 55, 56 and 57 (Appendix H.3): the AC energy production is very similar for the three orientations, around 128 kWh yearly for a basic 100 kW plant, testifying that the azimuth angle loses relevance with such high tilt values because of the sun's low path in the sky, the high proportion of diffuse radiation, and the balanced exposure to reflected light across all directions. [23]

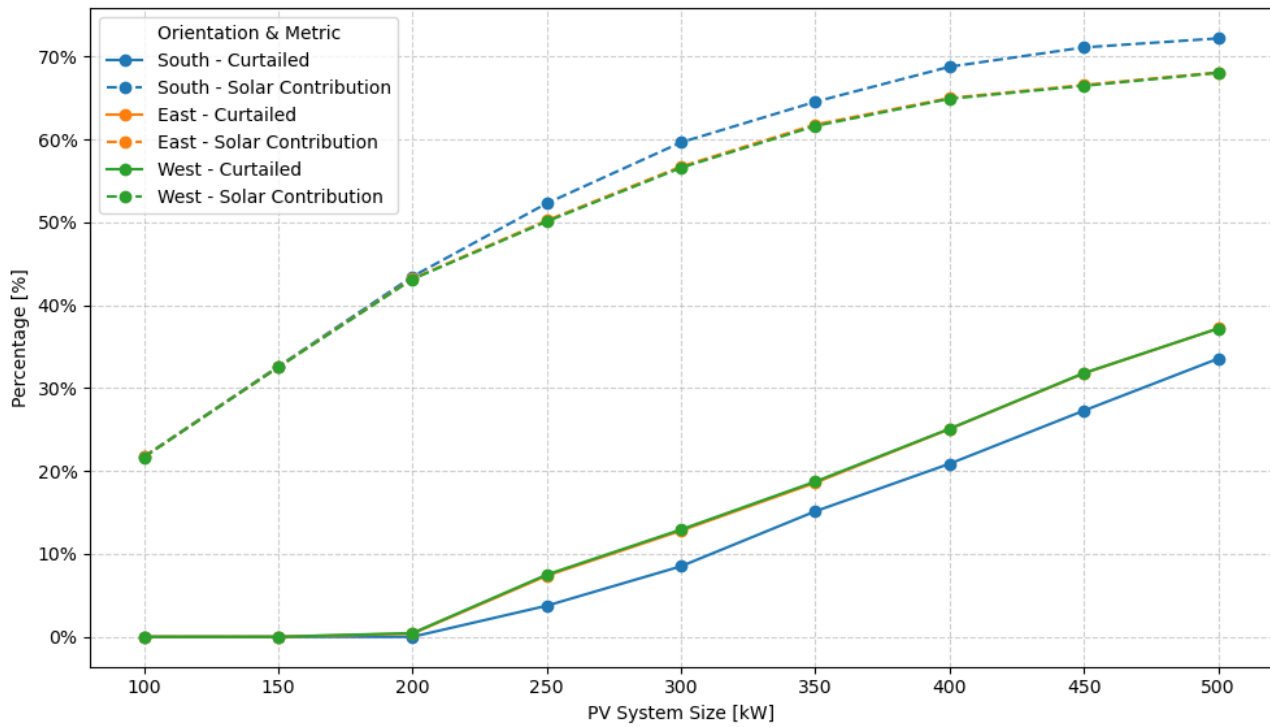


Figure 23: Growth trend of curtailed energy and solar contribution in Ilimanaq with increasing PV capacity.

Bifacial panels, vertical

Table 15: Curtailed Energy Percentage [%] by System Size [kW] and Orientation

Scenario	100 kW	200 kW	300 kW	400 kW	500 kW
South	0.0	0.0	8.5	20.9	33.6
East	0.0	0.4	12.8	25.1	37.2
West	0.0	0.5	12.9	25.1	37.2

The curtailed energy percentage graph shown in Figure 23 differs significantly from those previously reported. Notably, at a capacity of 200 kW, the curtailed energy percentage becomes slightly greater than zero. This is due to elevated production levels in May for the East- and West-facing systems, which marginally exceed local consumption during that month.

As illustrated in Figures 24, 25, 26, and in the figures provided in Appendix H.3, East- and West-oriented systems demonstrate higher energy output during the spring and summer months. In contrast, South-facing systems yield more in February, March, September, and October. However, this seasonal advantage does not lead to additional curtailment, as the generation in those months remains below the consumption threshold.

Combining this insight with the relatively lower output of South-facing systems during the summer months—when consumption is consistently exceeded for all orientations—results in a lower overall curtailed energy percentage for the South-facing configuration across all capacities.

The trend in solar contribution mirrors the pattern discussed earlier in Section 4.1, with an initial linear increase followed by a slowdown as curtailment rises. Despite the nearly identical total energy production across orientations (see Appendix H.3), the higher excess generation in East- and West-facing systems leads to reduced total displaced energy (Figure 22) and a lower solar share.

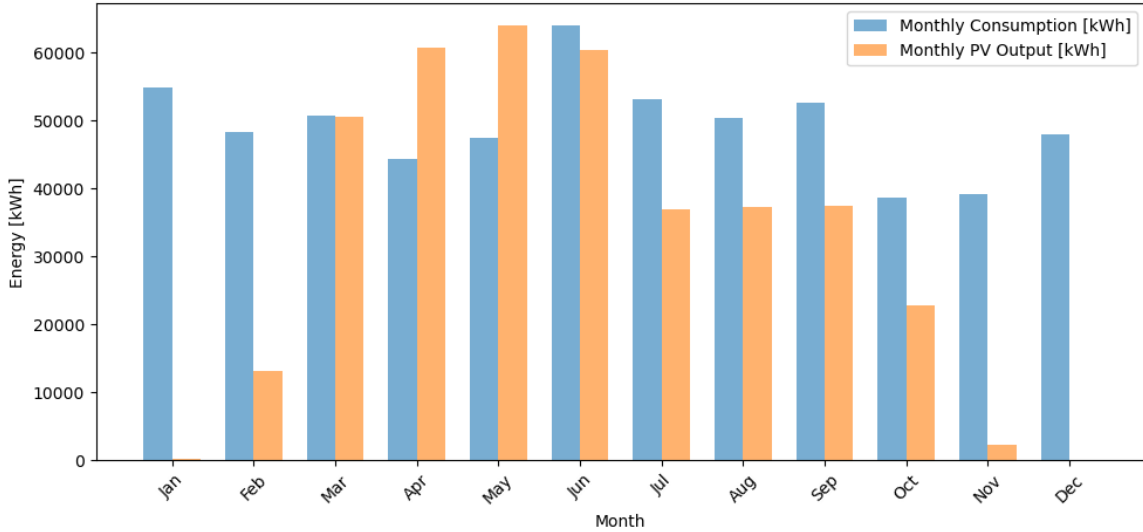


Figure 24: Monthly comparison of PV energy production and the Ililamaq energy consumption.
Bifacial panels, vertical, azimuth = 180°

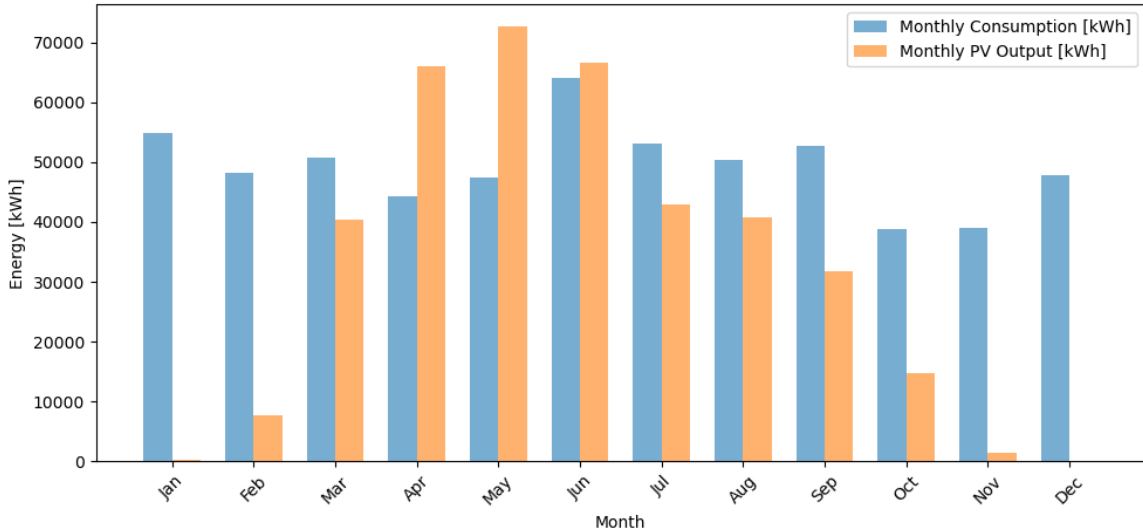


Figure 25: Monthly comparison of PV energy production and the Ililamaq energy consumption.
Bifacial panels, vertical, azimuth = 90°

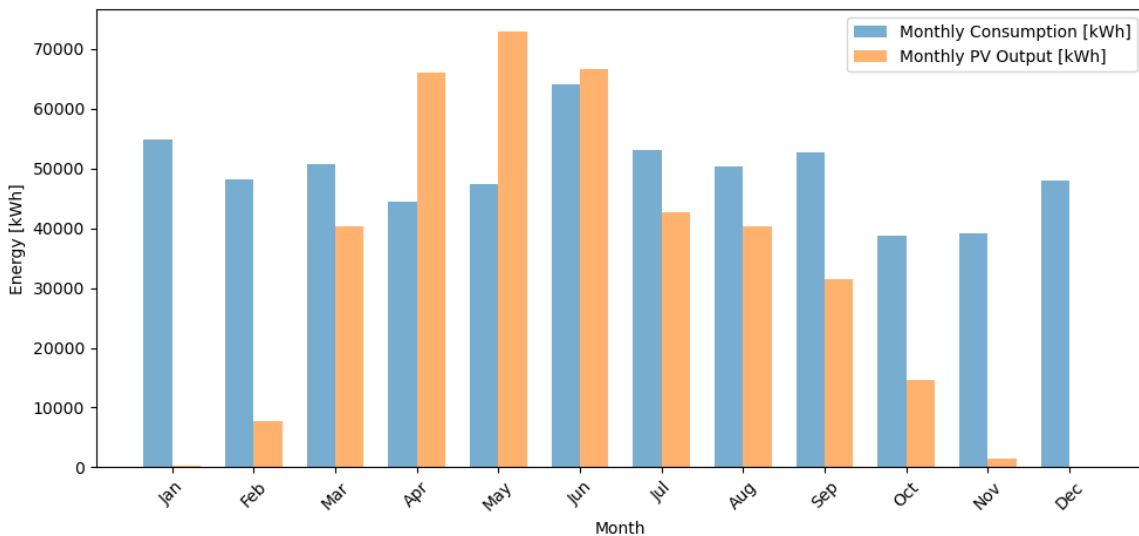


Figure 26: Monthly comparison of PV energy production and the Ilimanaq energy consumption.
Bifacial panels, vertical, azimuth = 270°

4.3 Monofacial panels

After the production analysis of bifacial plants, the focus moves to roof-mounted monofacial panels. This scenario is needed to simulate the installation of roof-mounted panels instead of ground-mounted systems.

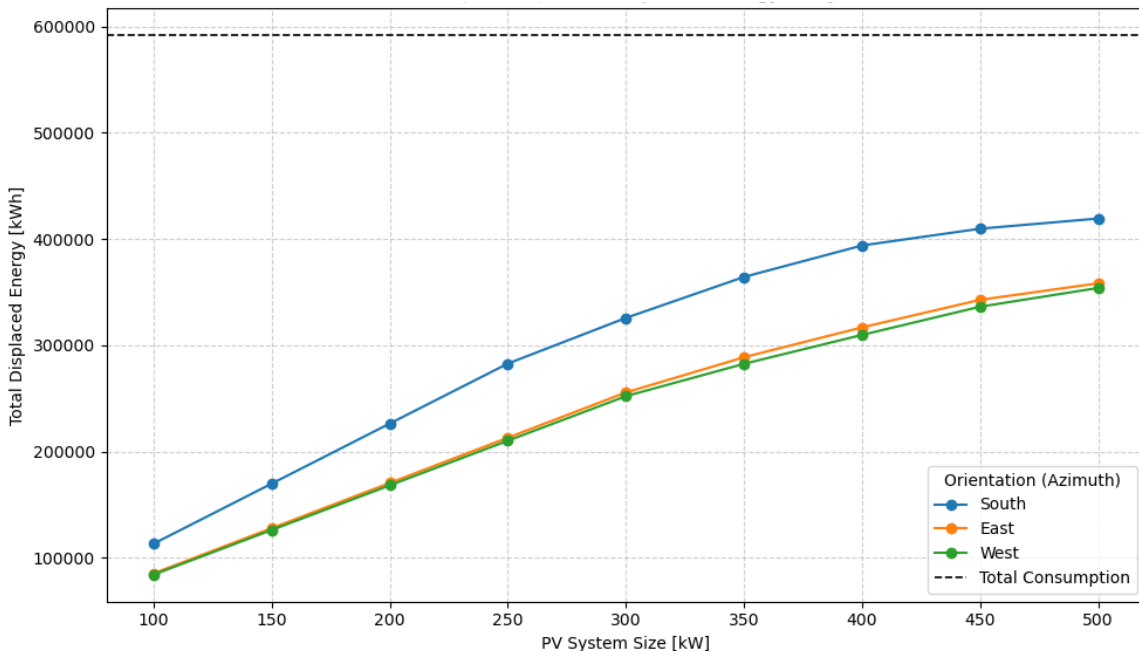


Figure 27: Growth trend of the displaced energy in Ilimanaq with increasing PV capacity.
Monofacial panels, tilt = 40°

Table 16: Annual displaced energy [MWh] for different system sizes and orientations.
Monofacial panels, tilt = 40°

Scenario	100 kW	200 kW	300 kW	400 kW	500 kW
South	113.1	226.3	325.7	393.9	419.3
East	85.2	170.4	255.5	316.8	358.3
West	84.0	168.1	252.0	309.7	353.9

The growth in this case keeps a linear trend for longer than for bifacial panels, because of the lower global production (shown in Appendix H.4) which needs a bigger capacity to get close to the consumption rate and consequently resulting into curtailment.

This also is the cause of a higher displaced energy increase from step to step, and then the curves tend to flatten later than in the previous cases, even more evidently for the East and West-facing scenarios.

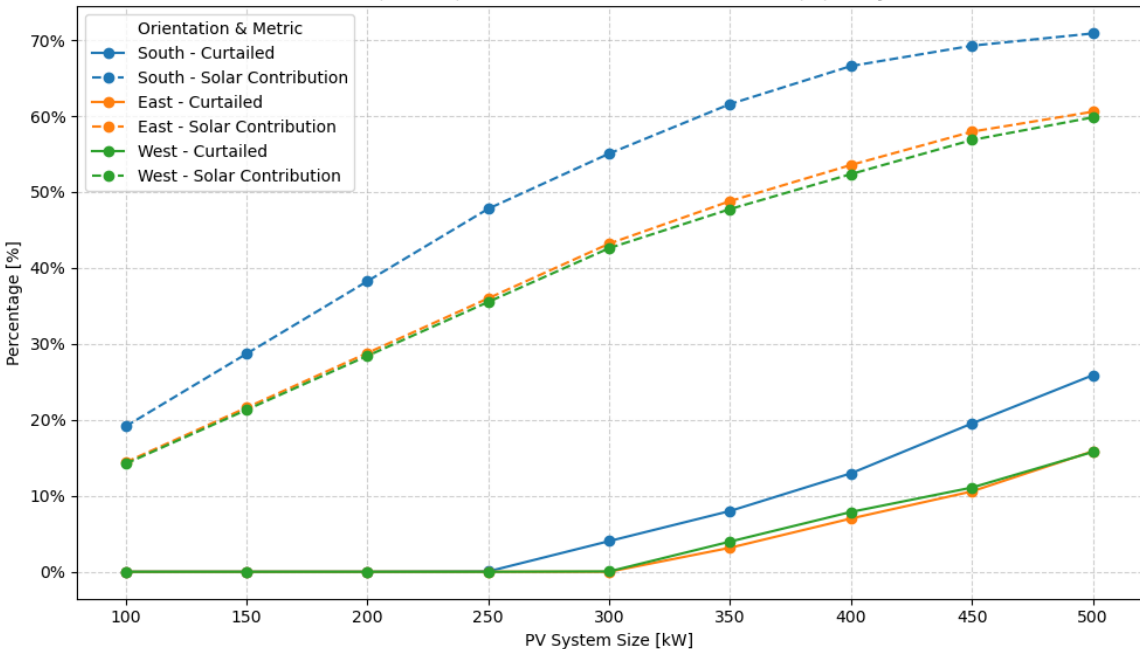


Figure 28: Growth trend of the displaced energy in Ilimanaq with increasing PV capacity.
Monofacial panels, tilt = 40°

Table 17: Curtailed Energy Percentage [%] by System Size [kW] and Scenario

Scenario	100 kW	200 kW	300 kW	400 kW	500 kW
South	0.0	0.0	4.0	13.0	25.9
East	0.0	0.0	0.0	7.0	15.9
West	0.0	0.0	0.0	7.9	15.8

Figure 28 and Table 17 confirm the observations discussed above: as expected, the curtailed energy

percentages are lower for all three monofacial scenarios compared to the previously analyzed bifacial ones.

Another key difference is that the curtailed energy shares are consistently higher for the 180° azimuth compared to the 90° and 270° orientations. While South-facing systems (azimuth of 180°) still benefit from a more favorable monthly production distribution—particularly in March, September, and October—the high curtailment observed during peak-irradiance months cannot be offset by this seasonal balance.

Moreover, unlike in the bifacial scenarios, the intermediate capacities—where the 180° azimuth previously benefited from a more even production profile—now result in relatively low energy outputs for the 90° and 270° orientations, which are insufficient to outperform the South-facing setups in overall energy production. This behavior can be observed in Figures 29, 30 and 31 below.

The solar contribution continues to follow the trend of the displaced energy. In this case as well, the curve begins to flatten at around 70% for the South-oriented system, while it stabilizes at approximately 60% for the East- and West-facing scenarios.

It is worth noting that the yellow and green dashed lines—representing East and West orientations, respectively—exhibit a steeper slope compared to the South-facing line. This is due to their lower overall production and curtailed energy shares, which makes the smoothing effect less pronounced.

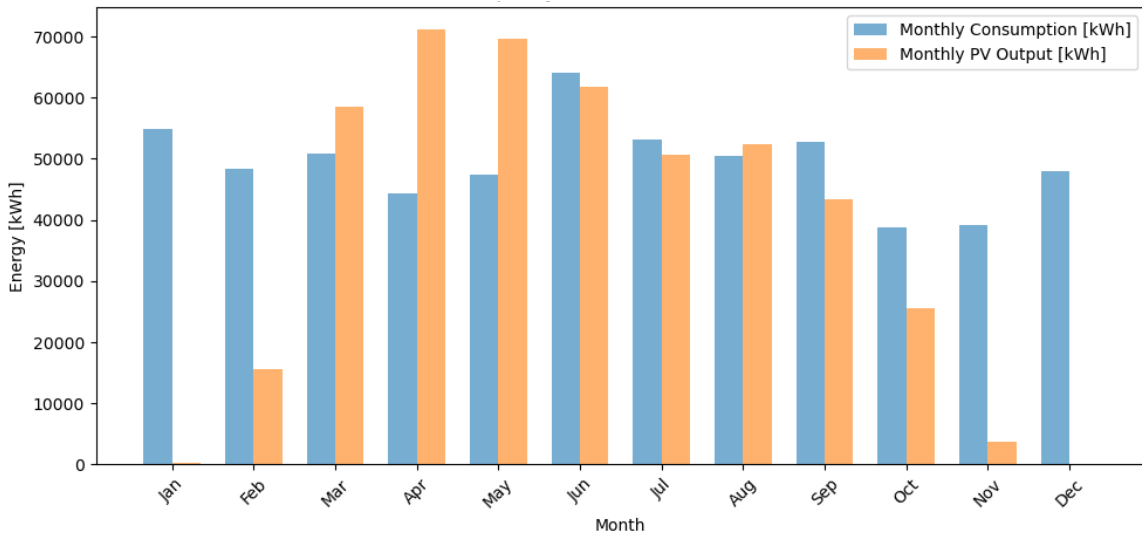


Figure 29: Monthly comparison of PV energy production and the Ilimanaq energy consumption.
Monofacial panels, tilt = 40° , azimuth = 180°

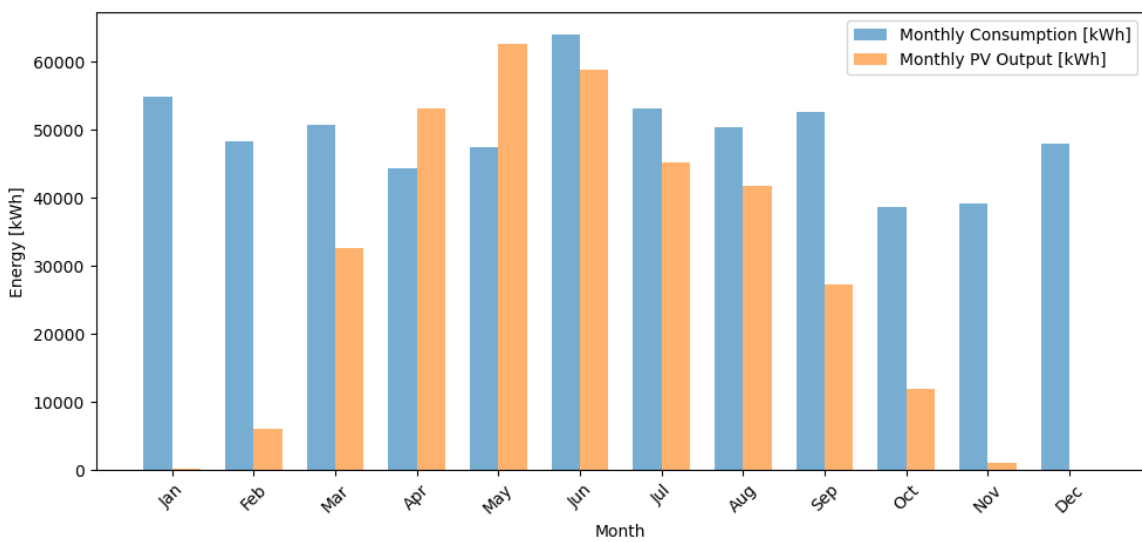


Figure 30: Monthly comparison of PV energy production and the Ililamaq energy consumption.
Monofacial panels, tilt = 40°, azimuth = 90°

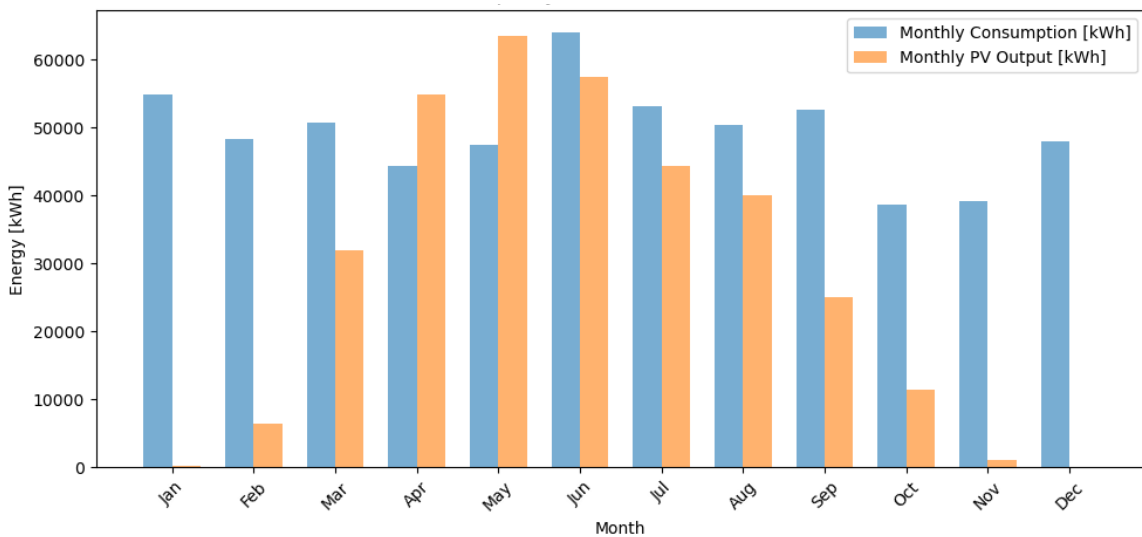


Figure 31: Monthly comparison of PV energy production and the Ililamaq energy consumption.
Monofacial panels, tilt = 40°, azimuth = 270°

4.4 Emissions reduction

The last step of the process involves studying how the intensive development of PV technologies can affect the CO₂ emissions of Ililamaq and, generally, of the whole Greenland, and in what scale this solution has the potential to reduce the carbon footprint of the island. The calculation made to compute the saved CO₂ emissions is a product between the displaced energy, obtained as shown in Section 4, and the emission factor of 0.807 $\frac{kgCO_2}{kWh}$. The reason for this choice is explained below, in Section 4.4.1. From this premise, it is easily deduced that the avoided emission follows the trend shown in the displaced energy plots: an initial fast linear increase, which is succeeded by a growth deceleration due to the always increasing share of curtailed solar energy caused by the augmenting mismatch between production and local consumption.

4.4.1 Emission factor

In order to assess the emission reduction potential, it is necessary to establish an emission factor, namely a coefficient linking the generation of electricity to a mass of produced CO₂ per energy unit. Nukissiorfiet, the Greenlandic energy entity, provided on their latest annual report emission factors specific for all the island's settlements, for both electricity and heat generation. [10] These estimated values vary from place to place, and are results of an evaluation based on the geography of the settlement, its proximity to the hydropower plants and historical data.

For Ililamaq in particular, it is estimated that the production of 1 kWh of electric energy requires 0.303 liters of oil, resulting in an emission factor of 0.807 $\frac{kgCO_2}{kWh}$.

4.4.2 Saved emissions results and discussion

The following section presents a detailed analysis conducted separately for each orientation, aiming to highlight performance variations across configurations.

Carbon dioxide reduction values are found multiplying the emission factor by the values of the displaced energy values reported in the tables of Section 4. The resulting plots naturally have the same shape of the curves shown in the displaced energy figures and because of this, to avoid repetitiveness, the plots are omitted and only the resulting values are reported in the tables below.

Table 18: Saved CO₂ [tons] by System Size [kW] and Orientation
Bifacial, 60° tilt

Scenario	100 kW	200 kW	300 kW	400 kW	500 kW
South	109.9	219.7	297.9	333.7	344.7
East	101.6	203.2	269.3	309.4	324.2
West	101.3	202.5	267.6	308.3	322.9

Table 19: Saved CO₂ [tons] by System Size [kW] and Orientation
Bifacial, vertical

Scenario	100 kW	200 kW	300 kW	400 kW	500 kW
South	103.8	207.5	284.8	328.4	344.7
East	103.5	206.3	270.9	310.3	325.1
West	103.4	206.0	270.2	309.9	324.8

Table 20: Saved CO₂ [tons] by System Size [kW] and Orientation
Monofacial, 40° tilt

Scenario	100 kW	200 kW	300 kW	400 kW	500 kW
South	91.3	182.6	262.8	317.9	338.4
East	68.7	137.5	206.2	255.7	289.2
West	67.8	135.7	203.4	249.9	285.6

For bifacial South-facing systems (Tables 18 and 19), the 60° tilted option provides the bigger CO₂ savings for every capacity until 500 kW are reached, when the vertical setup equalizes the 344.7 tons of the first scenario. East and West facing systems have instead slightly higher amounts of avoided emissions in the vertical scenario.

Monofacial roof-mounted systems, instead, obviously have a lower avoided emission mass for low capacities, for all the orientations. Looking at the 100 kW case, the saved CO₂ with a monofacial system is 16.9% lower than the obtained values with a tilted bifacial system, and the percentage difference grows to 32.4 and 33.1% for East and West facing systems respectively.

Similar values can be found when the savings of a roof mounted systems are compared to vertically ground-mounted systems: 12.0%, 33.6% and 34.3% for South, East and West, namely.

These values highlight the big performance gap that roof-mounted systems suffer from specially when facing East or West. Considering South-facing systems only, the differences thin out when capacities grow, as an effect of the high curtailments that bifacial systems are subjects to, unlike roof-mounted systems that experience lower waste.

The high curtailed energy shares however suggests to adopt a lower capacity, to avoid energy waste in a scenario in the absence of storage technologies.

From this perspective, the desirable approach is to reduce the waste of produced energy to the minimum, hence following the 200 kW scenario for bifacial systems, for both tilted and vertical solutions, leading to an average annual displaced energies amounts of 257 MWh for the three orientations and the two setups. The saved CO₂ in Ililamaq would, in this scenario, reach a yearly average of approximately 210 tons. South-oriented systems are to be preferred if the chosen solution are 60° tilted panels, while vertically installed modules are equally efficient when facing towards the three orientation and, in particular, is advisable to choose them instead of tilted panels for systems facing East and West, given the highest emissions savings, although by just a few tons. Another solution regarding tilted panels is the possibility to combine East and West facing panels: a common alternative to the more classic

single-standing panel consists into combining modules facing diametrically opposite directions into "hut-shaped" panels that grant a better total irradiation per land area.

Assuming that the overall yearly consumption of 591.6 MWh reported in Section 3.2 is exclusively diesel-based, the yearly emission of the baseline case would be 478 tons of CO₂; assuming the application of the best case scenario (South-facing panels, 60° tilted panels, 200 kW plant) which has an output of 272 MWh/y and 219.7 saved tons of CO₂, finally the result would be a 46% yearly emissions reduction compared to the initial case with a completely missing renewable integration.

Averaging the values for bifacial and 60° tilted panels and for the three azimuths because of their similarity, the average saved carbon emissions amount to approximately 210 tons, corresponding to a reduction of 44% compared to the baseline case.

For roof-mounted system there is instead the possibility to extend the installed capacity to 300 kW, when the curtailed energy share is null for East and West, and very low for South oriented systems, and can be a more economically feasible solution, given the cheapest installation costs, as they utilize existing infrastructure and involve a lower upfront investment [24], while the price of the panels themselves, which are comparable for the different technologies.

The economical benefit can be attractive for public investments, in spite of lower production, displaced energy and consequently also avoided emissions.

However, this advantage hides the drawback of space limitations that roof-mounted technologies are subject to, since the roof of a house typically can just host modules up to capacities of approximately 5 up to 20 kW, in more urbanized areas than Greenlandic settlements, which could mean an even lower capacity installed per-roof.

Also given the low concentration of buildings in Ililamaq and in Greenlandic settlements, the suggestion is to then adopt roof-mounted panels as a complementary solution to bifacial modules, that can be installed without the same spacial concerns that affects the monofacials.

4.4.3 Potential for electric heating

A further consideration can be made regarding the potential adoption of photovoltaic technologies for heating purposes. In Greenland, in 2023, 1299 TJ of diesel were consumed in households, the equivalent of 360 GWh, and 95 kton of CO_{2eq} were emitted consequently from this utilization, in the face of an overall emission 482.6 kton due to diesel combustion, across all sectors.[9] [25]

Within the 360 GWh, besides oil used for electricity generation, is also embedded the oil used for heating purposes. Even though Statistics Greenland does not provide the shares of oil used for the different purposes in households, it is possible to argue that a major percentage of the fuel is burnt for heating domestic spaces, rather than for generating electricity, since the Arctic climate imposes a high heating demand for much of the year, making oil-fired boilers and stoves the primary energy end-use in households.

In this context, over-sizing local ground-mounted PV plants could prove beneficial by enabling the use of surplus electricity to power electric boilers.

Rather than being curtailed, the excess generation could be redirected to heat domestic water, offering a more sustainable alternative to diesel-based heating. This approach could significantly contribute to

reducing household-related emissions on the island.

In the Ililamaaq case, the bifacial plant (with 60° tilted or vertical modules, depending on the orientation) could exceed 200 kW, if the excess energy was repurposed for electric heating. However, realizing this potential requires not only technological adaptation but also a transformation in energy consumption habits.

Transitioning from oil-based to electricity-based heating systems entails the adoption of new technologies—such as high-efficiency electric boilers or heat pumps—as well as a cultural shift in how energy is used and perceived by the local population.

The success of such a transition depends on raising awareness of the environmental and economic benefits, improving access to suitable electric heating technologies, and ensuring that energy infrastructure can support this change in demand patterns.

5 Conclusion

The objective of this thesis was to study the impact that a large-scale implementation of solar power technologies could have on the decarbonisation of the Greenlandic electric energy generation and carbon emissions

Before proceeding with the conclusion, it is important to highlight a major limitation of this study, namely its focus being exclusively on electricity generation, without considering other major energy demands in Greenland such as heating. Since heating constitutes a significant share of the country's overall energy consumption and associated emissions, future work should aim to integrate both electricity and thermal energy sectors for a more comprehensive decarbonisation assessment.

The motivations behind this choice reside in the high reliance the island has on diesel generators to produce electricity, specially in the settlements located far from one of the five hydropower plants built on the territory and supply just a few of the many towns and villages situated all along the coast and whose electric power production totally depend on the combustion of fossil fuels. For this reason, the study moves from simulations and models tailored for scenarios of PV adoption by small settlements, with the future auspice to scale them to a wider scale.

The starting point of the project was ground-measured data, obtained via DMI, of the GHI of six different weather stations in Greenland. After being analyzed, cleaned and filtered thanks to a thorough quality control process aiming to empty the dataset from imperfections and errors due to instrumental malfunctioning due to electronic or weather-related issues, the clean dataset was then used as a base for the comparison of two reanalysis datasets, ERA5 and NASA POWER, both available online. The reanalysis datasets of all the six stations were confronted with the DMI one, and the resulting RMSEs and biases have indicated ERA5 as the better fitting among the two.

The ERA5 dataset of Ilimanaq, a 53 inhabitants settlement located on the Greenlandic West coast whose consumption data for 2023 was provided by Nukissiorfiit, is the base of the next step of the analysis, consisting in modeling and simulating the performance of a PV plant in the supra cited location, in the light of a yearly electricity demand amounting to 591.6 MWh.

Different variants of the model were created: ground-mounted bifacial panels tilted by 45° or 60°, ground-mounted bifacial vertical panels, and monofacial roof-mounted panels tilted by 40°.

The setups' performances have been simulated for three different orientations, South, East and West, and multiple plant capacities, the selected ones being all the multiples of 50 kW, from a minimum of 100 kW to a maximum of 500 kW, and the results have been compared to the consumption data mentioned above to compute displaced energy values and curtailed energy and solar contribution percentages, to gain insights about the usefulness of increasing the plant capacity as opposed to a constant consumption habitude.

The simulations proved that bifacial panels, tilted and vertical, have a linear growth trend until the size of 200 kW, when curtailed energy becomes higher than zero for the first time because of some of the monthly consumption values being lower than the AC output of the plant in the same month. A 200 kW capacity corresponds to a solar fraction of 46% for South facing systems, and 42.5% for the two other orientations when it comes to 60° tilted bifacial solutions. The percentages are between 43 and 43.5% for all the three azimuths in the vertical case. This behavior becomes more influent with

capacity increase, as testified by the deceleration faced by the growth speed of the displaced energy values, whose curve tends, in both cases, to flatten reaching approximately 430 MWh/y for a capacity of 500 kW, in a South-facing scenario, and approximately 400 MWh/y in East/West facing scenarios. Solar contribution is also similarly affected, assuming a similar curve trend and assessing itself around a share of 72%, for modules oriented toward South, and 68%, for the remaining orientations. This means that once 200 kW is exceeded, further increases in PV capacity result in rapidly diminishing returns in terms of solar contribution.

Saved emissions are computed multiplying the displaced energy values by an emission factor of $0.807 \frac{kgCO_2}{kWh}$, specific for Ilimanaq and obtained from the Nukissiorfiit's annual report for year 2023. [10] This calculation structure makes the avoided emissions have the same shape and trend as the displaced energy, being the factor a constant, hence they have a fast initial growth followed by a subsequent flattening when the capacity exceeds 200 kW.

In the absence of a storage technology, the approach of this project is to scale the plant up to a maximum of approximately 200 kW, to avoid excess production that can't be repurposed.

Before proceeding with further discussions, it is important to note that curtailment is not always negative. In fact, oversizing a solar plant can offer economic advantages: if the cost of solar electricity is lower than that of diesel-generated power, it may be economically justified to accept a certain level of curtailment. This allows for greater displacement of diesel consumption during sunny periods, even if some excess energy must occasionally be curtailed. However, the economic aspect in this project is secondary to the purely energy-related perspective and the curtailment-minimizing approach was preferred.

In the case of South facing panels, 60° tilted panels have a better output for this capacity, while East and West facing solutions find a better fit in the vertically-installed modules.

Without retaining the surplus electricity, oversizing the plant would require higher investments which would result in a lower efficiency, and this would add up with more economic losses related to the unsold curtailments.

On average, these solutions grant approximately 260 MWh of displaced energy yearly, corresponding to 210 saved tons of CO₂ and a 44% reduction of carbon emissions compared to the base scenario, without any renewable solutions integration. The reduction share grows until 46% if the adopted solution is the best case scenario, a 200 kW plant of South-facing 60° tilted panels.

Monofacial roof-mounted systems have, on the other hand, a higher curtailment limit (300 kW) compared to their counterpart, and lower installation costs linked to the usage of roofs as pre-existing mounting structures, but encounter the major disadvantage of having a much lower available mounting area compare to the bifacial alternative.

In Ilimanaq particularly, being a small settlement, the roof surface availability is too low to allow a large scale development of this technology, which is advised as a side solution for the few buildings of the village.

Nevertheless, it can't reach its potential, which is still high despite the lower energy production values which make it less affected by curtailments and allows the final displaced energy values to at least partially bridge the gap with its alternatives for a South facing 500 kW plant - 419 MWh/y against 427 MWh/y, curtailed shares of 26% against an average of 35% and 338 against 345 tons of saved

carbon emissions.

These answers confirm the good potential of a technology that is however necessarily limited in term of spacial availability, in a place like Greenland which is the least densely populated territory on Earth.

Curtailment could be avoided by repurposing surplus PV electricity for heating in Greenlandic households, where heating demand is high and largely met by diesel. In 2023, household diesel use reached 1299 TJ (360 GWh), contributing to 95 kton of CO₂ emissions.

Although precise usage breakdowns are unavailable, it is likely that most of this energy supported space heating due to the Arctic climate. Oversizing the Ilimanaq bifacial plant, which could exceed 200 kW, could allow excess generation to power electric boilers. This shift would reduce diesel reliance and emissions but requires not only technological upgrades, but also changes in consumer habits, infrastructure, and awareness.

Energy storage can be implemented as a repository for the excess generation occurring in spring or summer. Some potential solutions that have been investigated include battery energy storage (BES), mostly for diesel-off operations during the summertime, to garner surplus energy to be then released in low-radiation hours or days, for lightning, or heating purposes, as just mentioned in the paragraph above.

Integration of hydrogen to BES technologies has also been object of studies with the purpose to make batteries more suitable for seasonal storage because this implementation could enable opportunities for repurposing linked to the broader needs of the whole settlement, like desalination or district heating. [26]

Compared to hourly or daily balancing strategies, redirecting curtailed energy toward seasonal applications offers a greater potential for emission reductions and energy system optimization, although bigger investments and operational costs must be faced in this scenario. The better potential is because surplus generation in high-irradiance months — if stored or repurposed for long-term uses such as space heating or water desalination — directly offsets significant diesel consumption during the extended Arctic heating season.

A large scale implementation of storage technologies could then allow the expansion of the hypothesized ground-mounted plants, allowing both the figures of displaced energy and solar contribution to increase. The hope is of Nukissiorfít to opt for investments towards more renewable energy solutions in disconnected settlements and to accompany this choice with storage technologies that could improve their effectiveness.

Some last considerations must be made regarding the scalability of this project on a wider size, including all Greenland.

Given the vast land availability on the island's territory, and assuming the feasibility of retrieving consumption data for other towns and settlements, similar calculations and simulations to the ones made in this thesis can be replicated for other locations.

A scenario including all the Greenlandic settlements not connected to already existing hydropower plants, would entail variable consumptions and production profiles, due to the demand variability for each location and for the different solar resource availability between the southern and northern extreme latitudes of what's the biggest island in the world. Taking also into consideration the different emission factors that Nukissiorfít provide on their annual report [10], and that will maybe be updated in the

next publications, it can be absolutely possible to replicate what done in this study on a larger scale and make more accurate estimations of the emissions reduction impact for the whole Greenland.

The continuation of studies related to storage technologies and their integration into remote microgrids will be essential to ensure year-round reliability and maximize the use of solar energy. Future work should focus on evaluating the technical and economic feasibility of hybrid storage systems—such as battery and hydrogen-based solutions—for seasonal and daily balancing. Additionally, incorporating spatially resolved consumption data and refining solar resource assessments across the country would enhance the accuracy of PV system design and emissions impact evaluation. Altogether, these developments could pave the way for a more sustainable, decentralized energy transition across Greenland, tailored to the specific needs and conditions of each settlement.

References

- [1] World Meterological Organisation, “Global temperature is likely to exceed 1.5°C above pre-industrial level temporarily in next 5 years,” *wmo.int*, 2024.
- [2] NASA Earth Observatory, “World of change: Global temperatures,” *earthobservatory.nasa.gov*, 2024.
- [3] M. Rantanen, “The arctic has warmed nearly four times faster than the globe since 1979,” *Communications Earth & Environment*, 2022.
- [4] S. Jiang, A. Ye, and C. Xiao, “The temperature increase in greenland has accelerated in the past five years,” *Global and Planetary Change*, 2020.
- [5] K. Goto-Azuma, T. Homma, T. Saruya, F. Nakazawa, Y. Komuro, N. Nagatsuka, M. Hirabayashi, Y. Kondo, M. Koike, T. Aoki, R. Greve, and J. Okuno, “Studies on the variability of the greenland ice sheet and climate,” *Polar Science*, 2021.
- [6] T. Galimova, R. Satymov, D. Keiner, and C. Breyer, “Sustainable energy transition of greenland and its prospects as a potential arctic e-fuel and e-chemical export hub for europe and east asia,” *Energy*, 2024.
- [7] Naalakkersuisut - Government of Greenland, “Greenland hydropower resources,” 2024. Accessed: 2025-04-25.
- [8] A. Mustayen, M. Rasul, X. Wang, M. Negnevitsky, and J. Hamilton, “Remote areas and islands power generation: A review on diesel engine performance and emission improvement techniques,” *Energy Conversion and Management*, vol. 260, 2022.
- [9] Grønlands Statistik, “Energiforbrug 2023,” December 2024.
- [10] Nukissiorfiet, “Annual report 2023.” <https://nukissiorfiit.gl/da/om/Aarsregnskaber>, 2023. Appendix 2, Pages 66-67-68.
- [11] C. J. Cox and S. Morris, “The de-icing comparison experiment (d-ice): A campaign for improving data retention of radiometric measurements under icing conditions in cold regions: Science and implementation plan,” tech. rep., NOAA Earth System Research Laboratory (ESRL) Physical Sciences Division and CIRES, July 2017. Project Leads, CIRES and NOAA ESRL PSD.
- [12] J. T. Peterson, E. C. Flowers, and J. H. Rudisill, “Dew and frost deposition on pyranometers,” *Journal of Applied Meteorology*, vol. 12, no. 7, pp. 1231–1233, 1973.
- [13] A. R. Jensen and Y.-M. Saint-Drenan, “Quality assessment of solar irradiance data,” 2025. Accessed: 2025-04-27.
- [14] Weather Spark, “Climate and Average Weather Year Round at Danmarkshavn, Greenland,” 2025. Accessed: 2025-04-27.
- [15] C. E. Hartvig and M. Grønbek Bager, “Energilagring til Ililamaaq,” Master’s thesis, MARTEC (Maritime and Polytechnic University College) - in collaboration with Nukissiorfiet, 2023.

- [16] E. M. Tonita, A. C. Russell, C. E. Valdivia, and K. Hinzer, “Optimal ground coverage ratios for tracked, fixed-tilt, and vertical photovoltaic systems for latitudes up to 75°n,” *Solar Energy*, vol. 258, pp. 8–15, 2023.
- [17] N. Riedel-Lyngskær, M. Ribaconka, M. Pó, A. Thorseth, S. Thorsteinsson, C. Dam-Hansen, and M. L. Jakobsen, “The effect of spectral albedo in bifacial photovoltaic performance,” *Solar Energy*, vol. 231, pp. 921–935, 2021.
- [18] J. Eggeling, “Modeling albedo in the dry snow zone of the greenland ice sheet,” technical report, Lund University, Department of Physical Sciences, June 2014.
- [19] Weather Spark, “Climate and Average Weather Year Round in Nuuk, Greenland,” 2025. Accessed: 2025-05-18.
- [20] Weather Spark, “Climate and Average Weather Year Round in Ilulissat, Greenland,” 2025. Accessed: 2025-05-18.
- [21] N. Janotte, S. Wilbert, F. Sallaberry, M. Schroedter-Homscheidt, and L. Ramirez, “Principles of csp performance assessment,” in *The Performance of Concentrated Solar Power (CSP) Systems* (P. Heller, ed.), pp. 31–64, Woodhead Publishing, 2017.
- [22] R. E. Pawluk, Y. Chen, and Y. She, “Photovoltaic electricity generation loss due to snow – a literature review on influence factors, estimation, and mitigation,” *Renewable and Sustainable Energy Reviews*, vol. 107, pp. 171–182, 2019.
- [23] S. Jouttiäärvi, J. Thorning, M. Manni, H. Huerta, S. Ranta, M. D. Sabatino, G. Lobaccaro, and K. Miettunen, “A comprehensive methodological workflow to maximize solar energy in low-voltage grids: A case study of vertical bifacial panels in nordic conditions,” *Solar Energy*, vol. 262, pp. 1004–1012, 2023.
- [24] B. Samaila and J. M. Garba, “Comparative study on ground and roof-mounted solar pv systems,” *Journal of Energy Engineering and Thermodynamics*, vol. 4, Oct–Nov 2024.
- [25] Statistics Greenland, “Co2 emissions by industry (1990–2022),” 2024. Accessed: 2025-06-22.
- [26] A. Pantaleo, M. R. Albert, H. T. Snyder, S. Doig, T. Oshima, and N. E. Hagelqvist, “Modeling a sustainable energy transition in northern greenland: Qaanaaq case study,” *Sustainable Energy Technologies and Assessments*, vol. 54, p. 102774, 2022. Published under CC BY license.

Appendix

A Hydropower plants

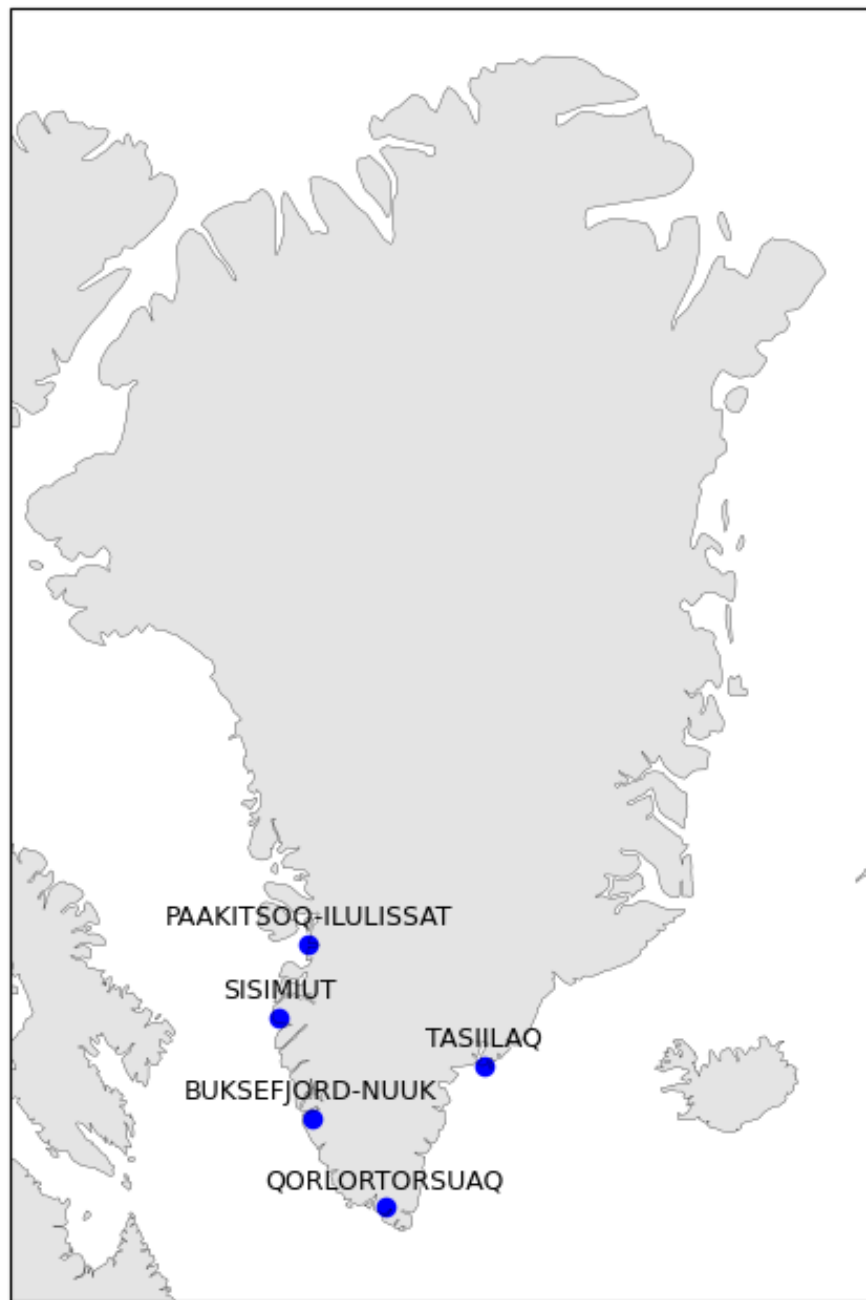


Figure 32: Map of the hydropower plants in Greenland

B Example of time step distribution for the Nuuk station

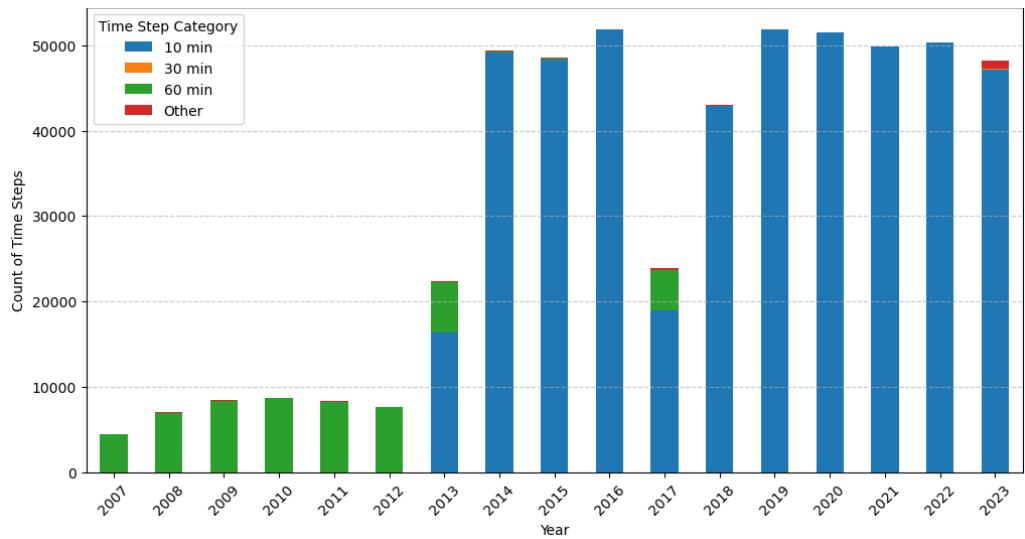


Figure 33: Time steps distribution for the Nuuk DMI station

C 2-D visualizations

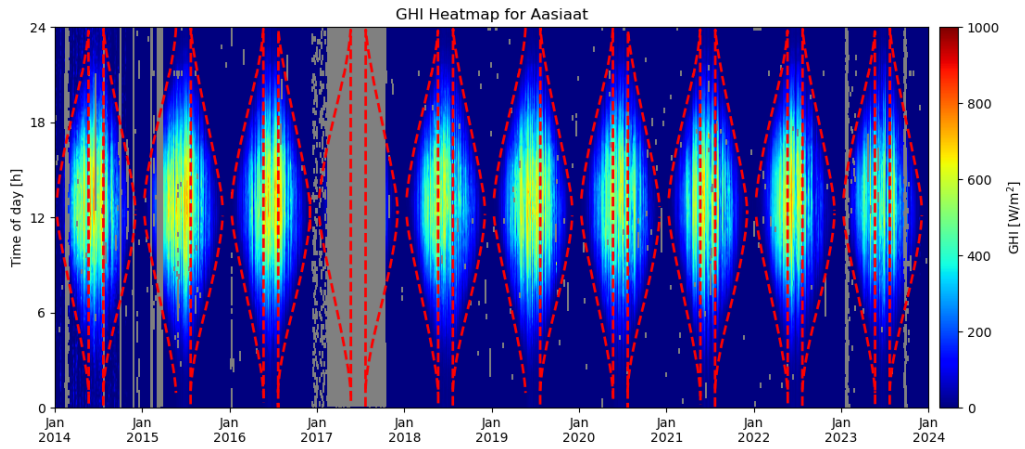


Figure 34: 2-D visualization of the raw data for Aasiaat

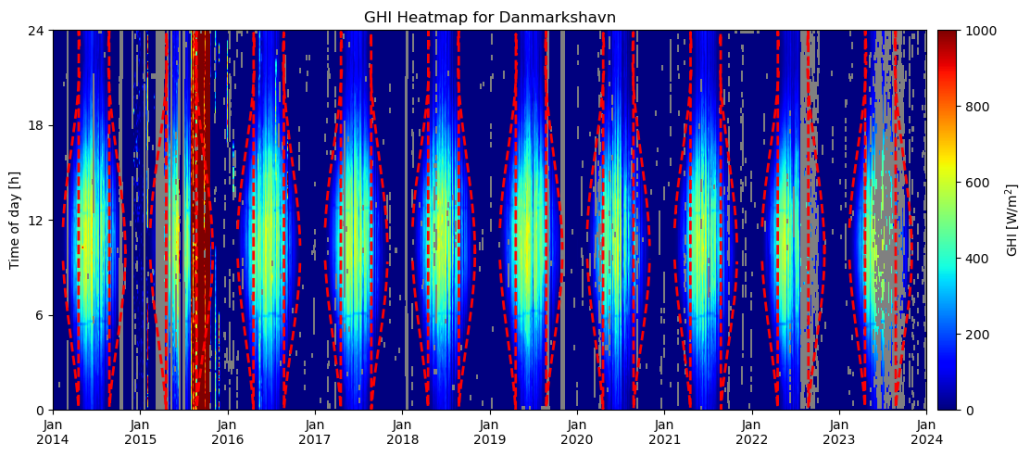


Figure 35: 2-D visualization of the raw data for Danmarkshavn

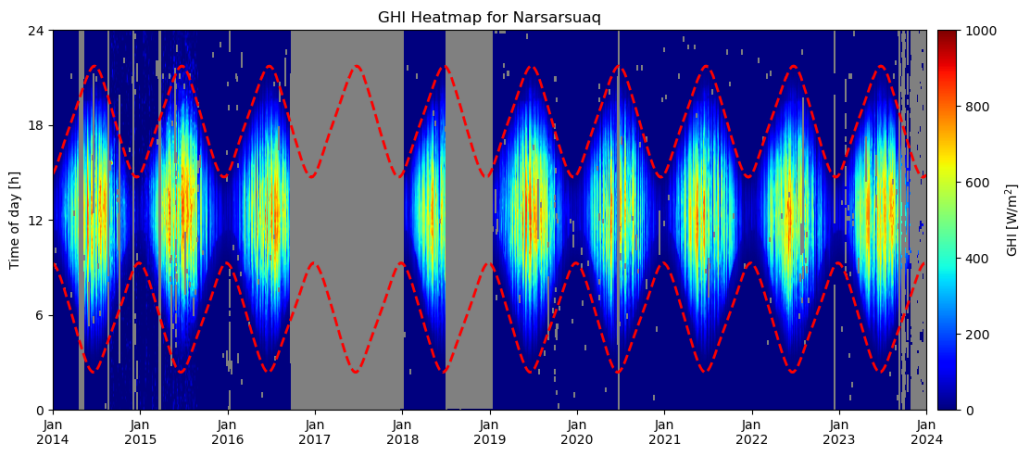


Figure 36: 2-D visualization of the raw data for Narsarsuaq

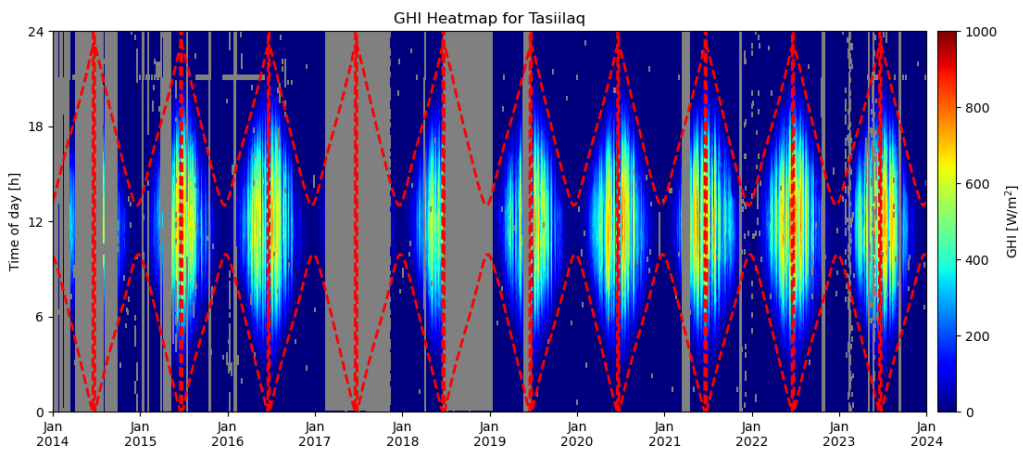


Figure 37: 2-D visualization of the raw data for Tasiilaq

D Additional data filtering

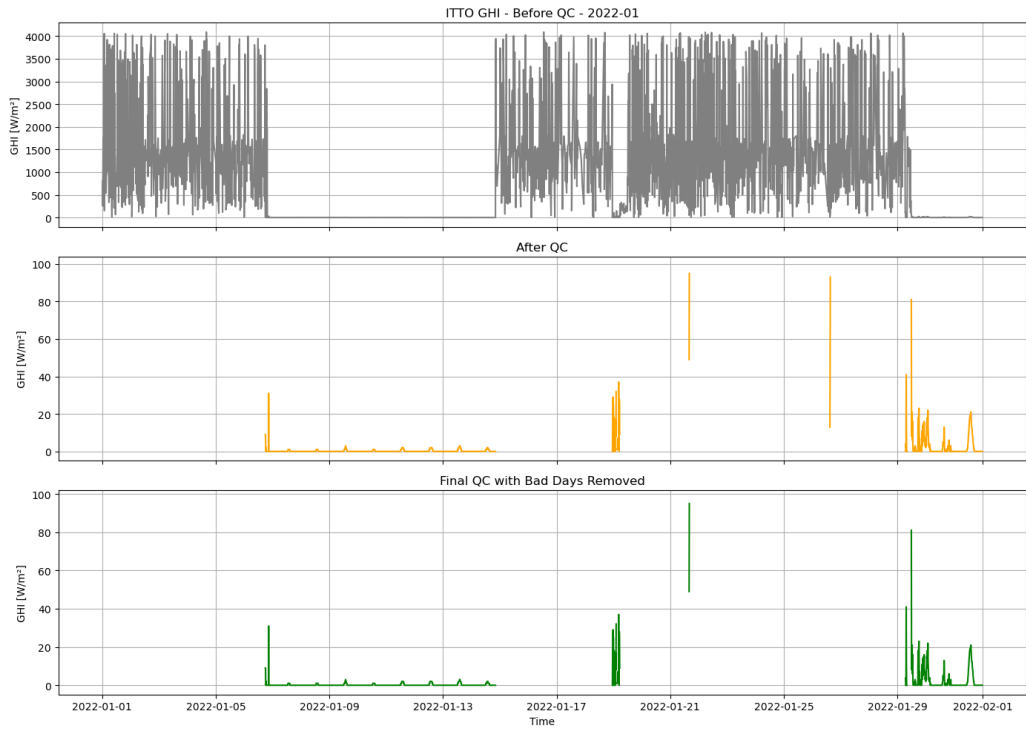


Figure 38: The three filtering steps shown for the month of January for the Ittoqqortoormiit station.

E Scatter plots

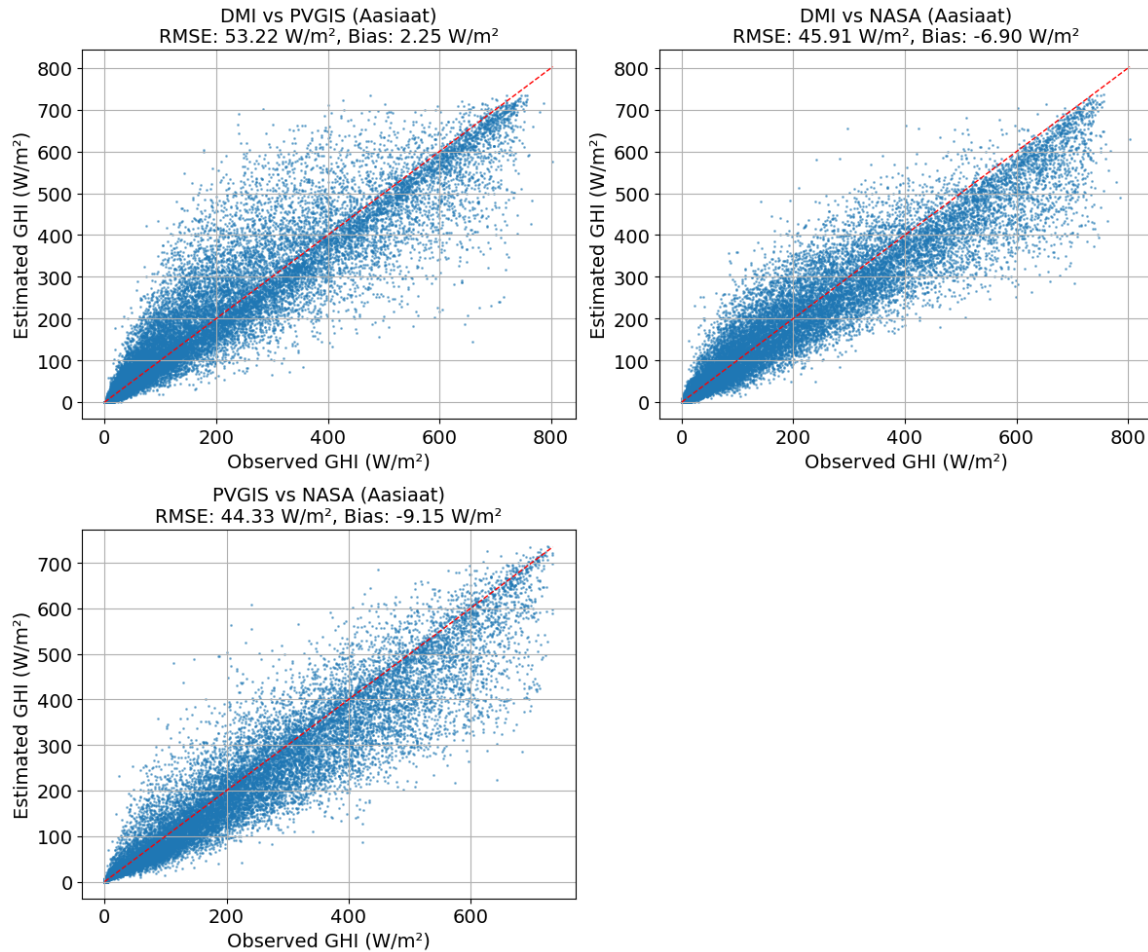


Figure 39: Scatter plot for Aasiaat

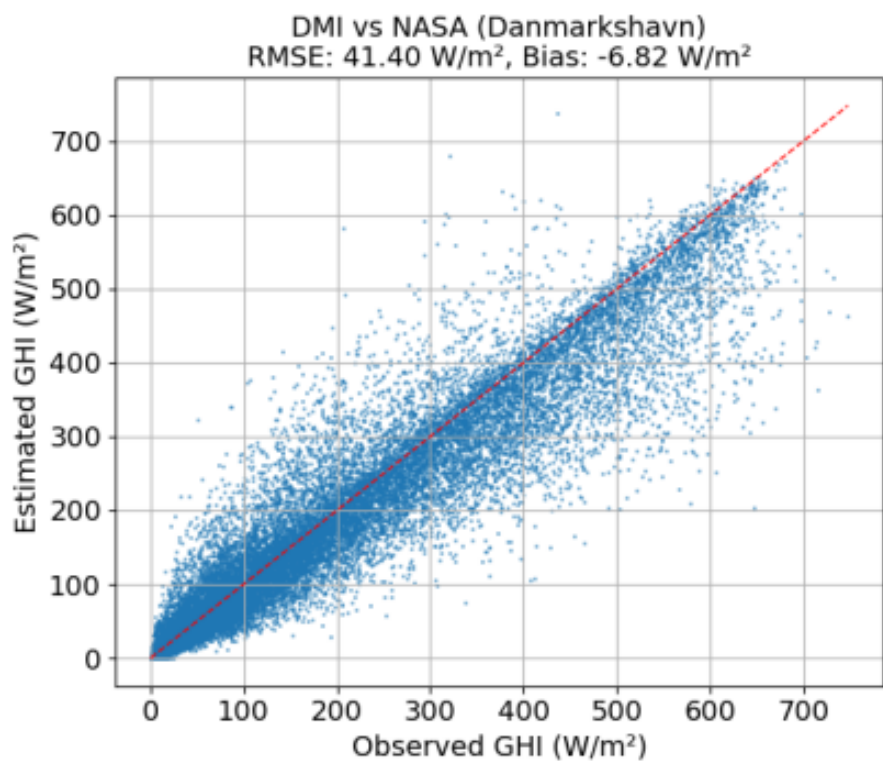


Figure 40: Scatter plot for Danmarkshavn

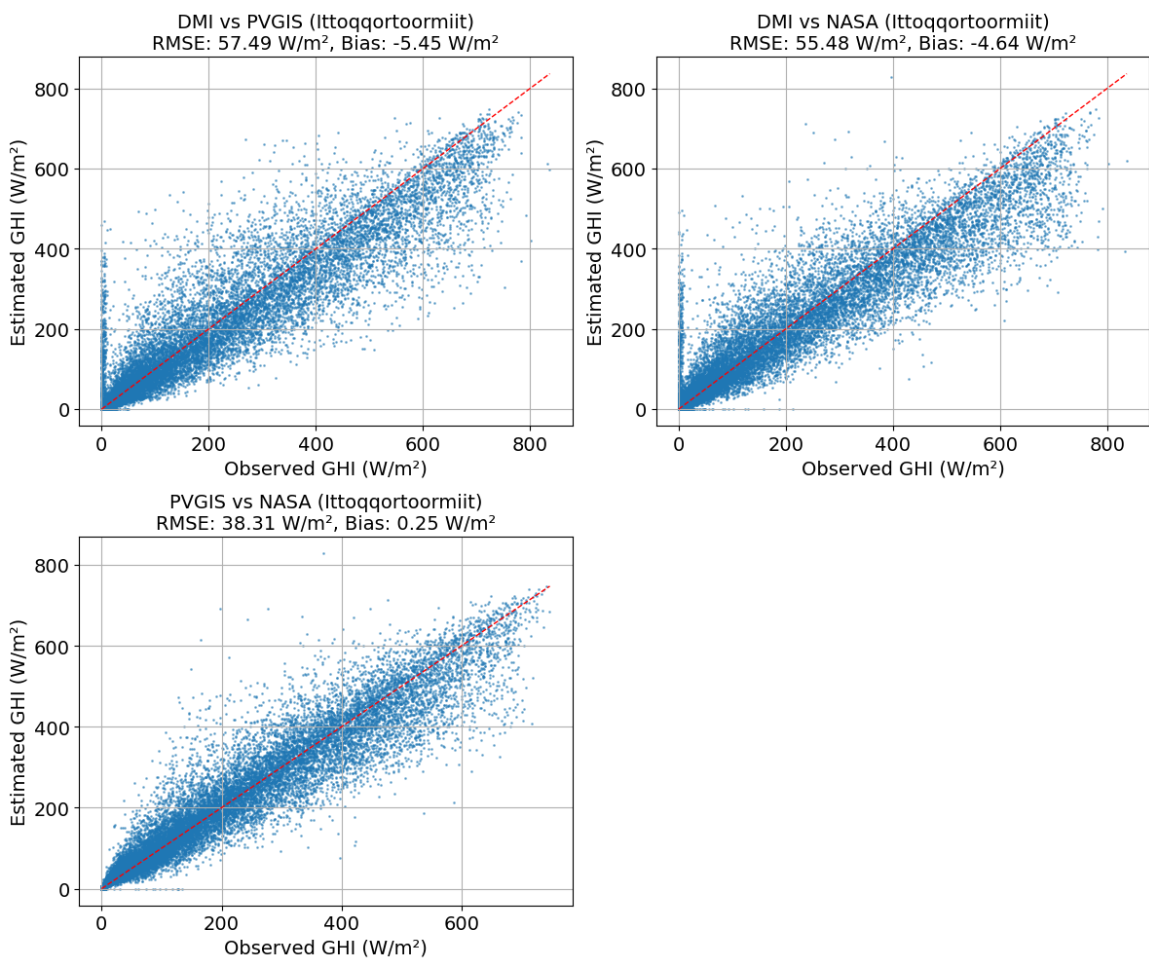


Figure 41: Scatter plot for Ittoqqortoormiit

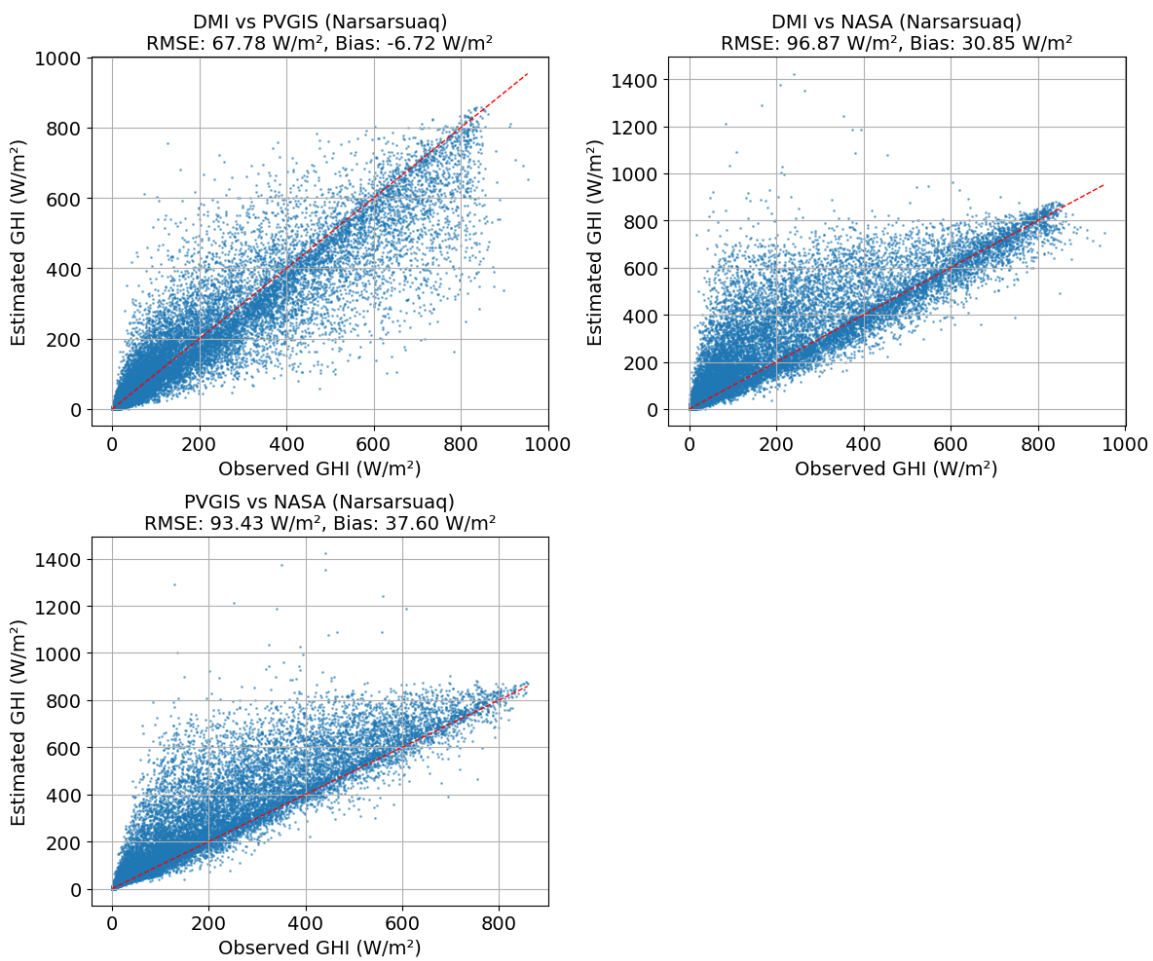


Figure 42: Scatter plot for Narsarsuaq

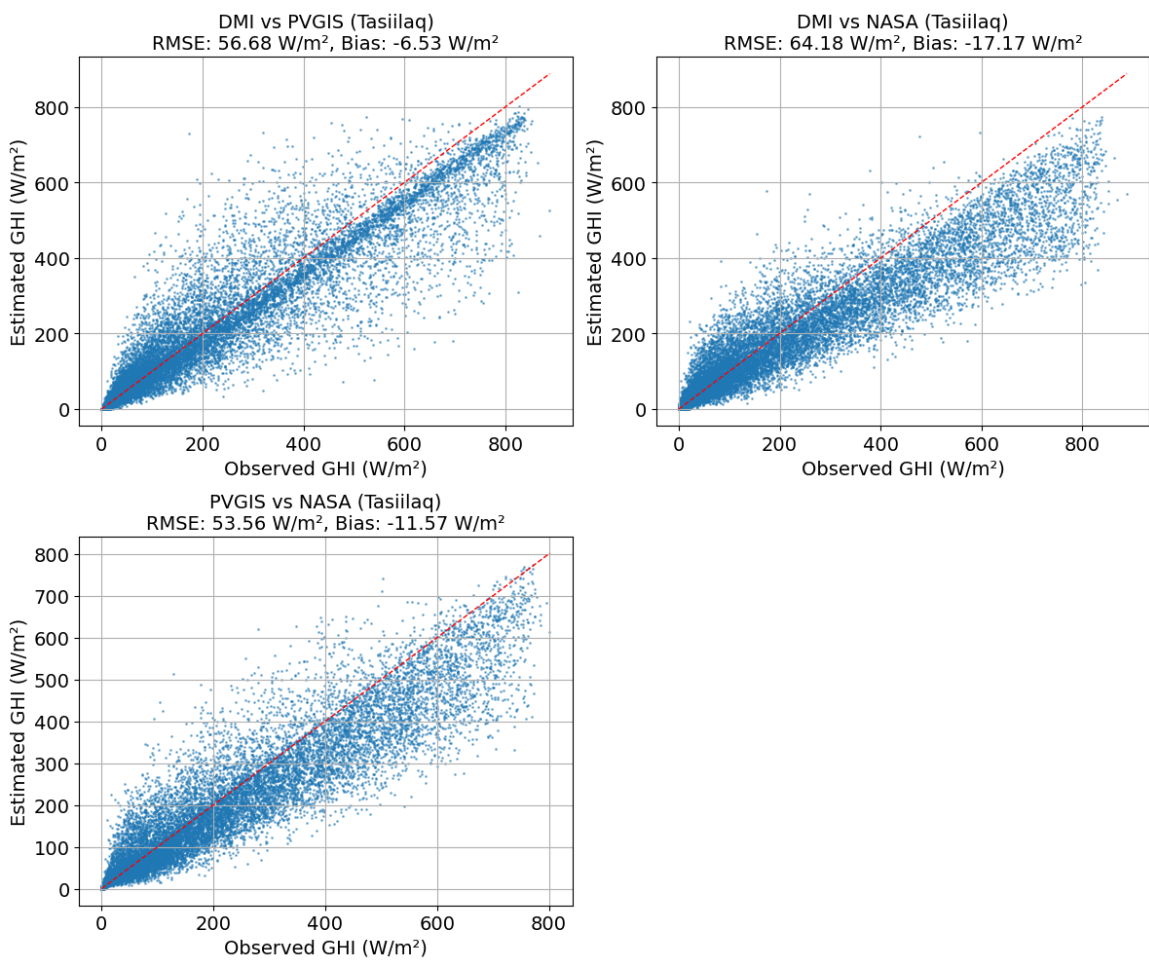


Figure 43: Scatter plot for Tasiilaq

F Location of the settlements of interest



Figure 44: Location of the settlements of interest

G Energy consumption in Ilimanaq and Qeqerarsuatsiaat

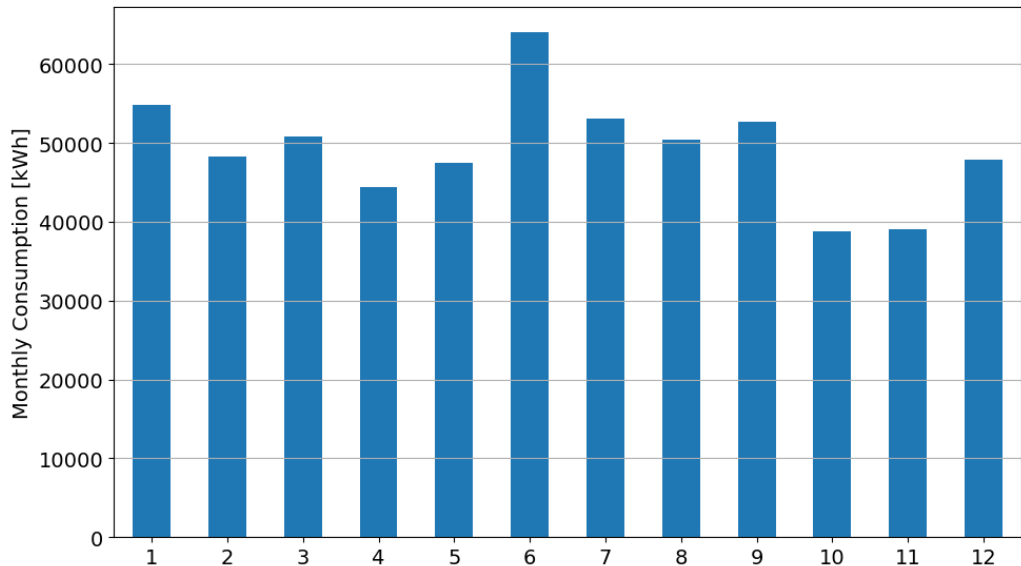


Figure 45: Monthly energy consumption in Ilimanaq

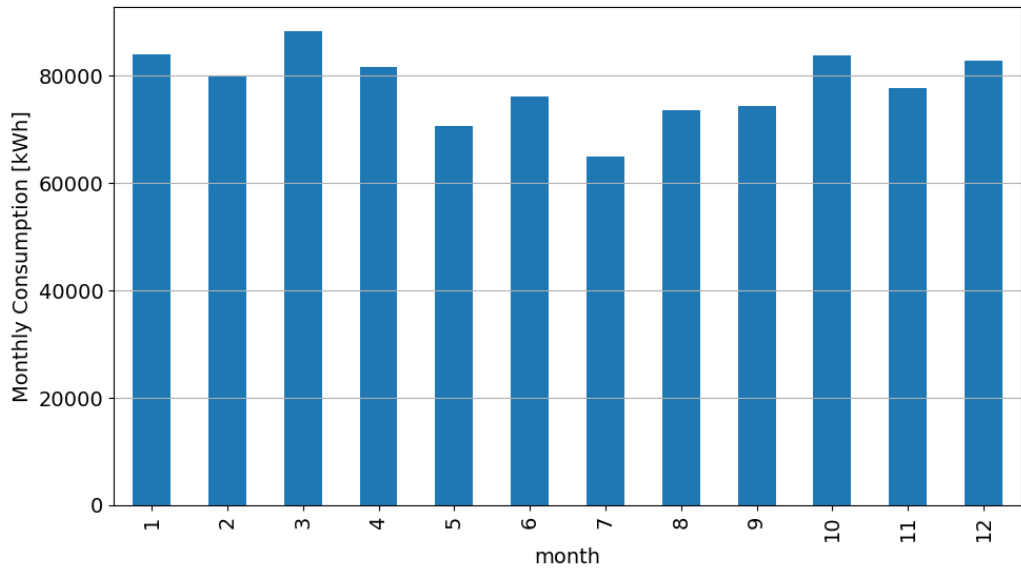


Figure 46: Monthly energy consumption in Qeqerarsuatsiaat

H PV Production

H.1 Bifacial panels, 60° tilt

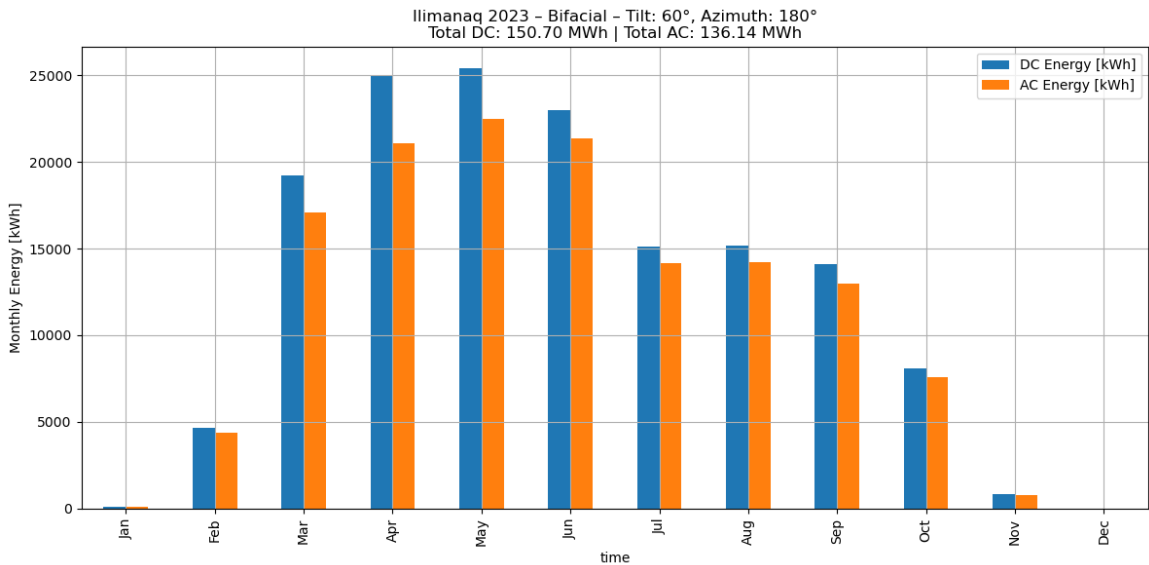


Figure 47: PV production in Ilimanaq in 2023, bifacial 100 kW plant
Tilt = 60°, South facing

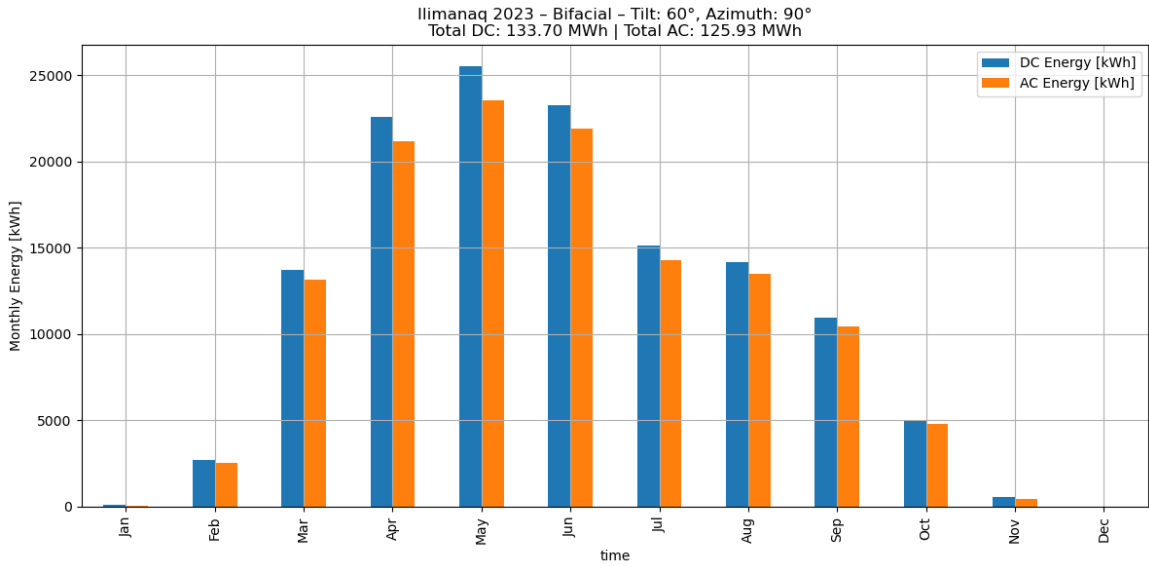


Figure 48: PV production in Ilimanaq in 2023, bifacial 100 kW plant
Tilt = 60°, East facing

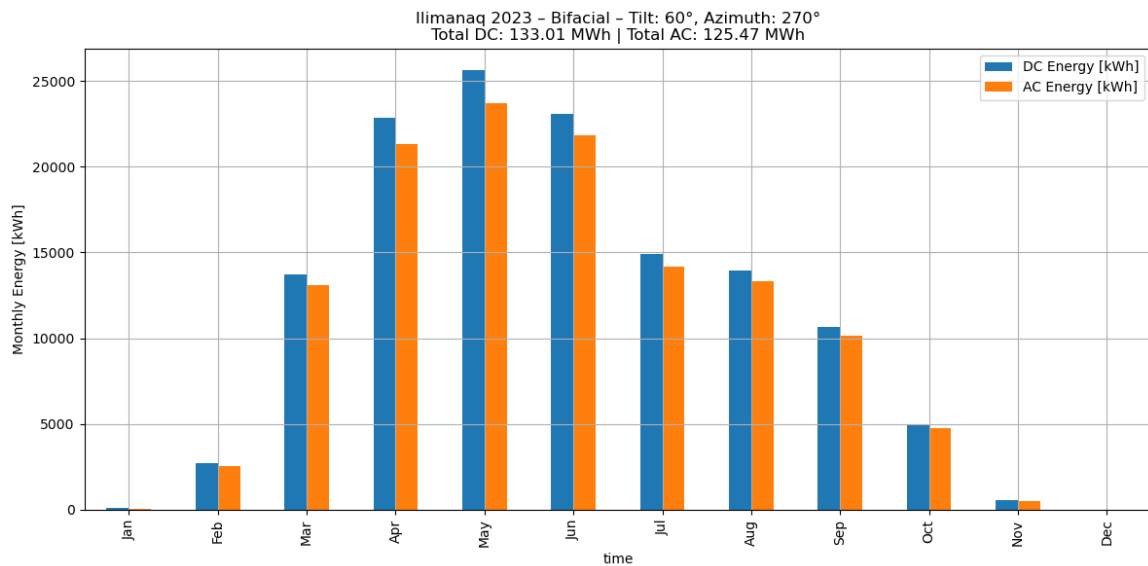


Figure 49: PV production in Ilimanaq in 2023, bifacial 100 kW plant
Tilt = 60°, West facing

H.2 Bifacial panels, 45° tilt

Below is reported the analysis conducted for 45° bifacial panels, that was initially meant to be part of the analysis but was consequently discarded for not adding much value to the work compared to the 60° tilted case.

It is, however, still reported for the interesting behavior retraceable in the curtailed energy at 200 kW, whose analogies and differences with the 60° tilt case are reported.

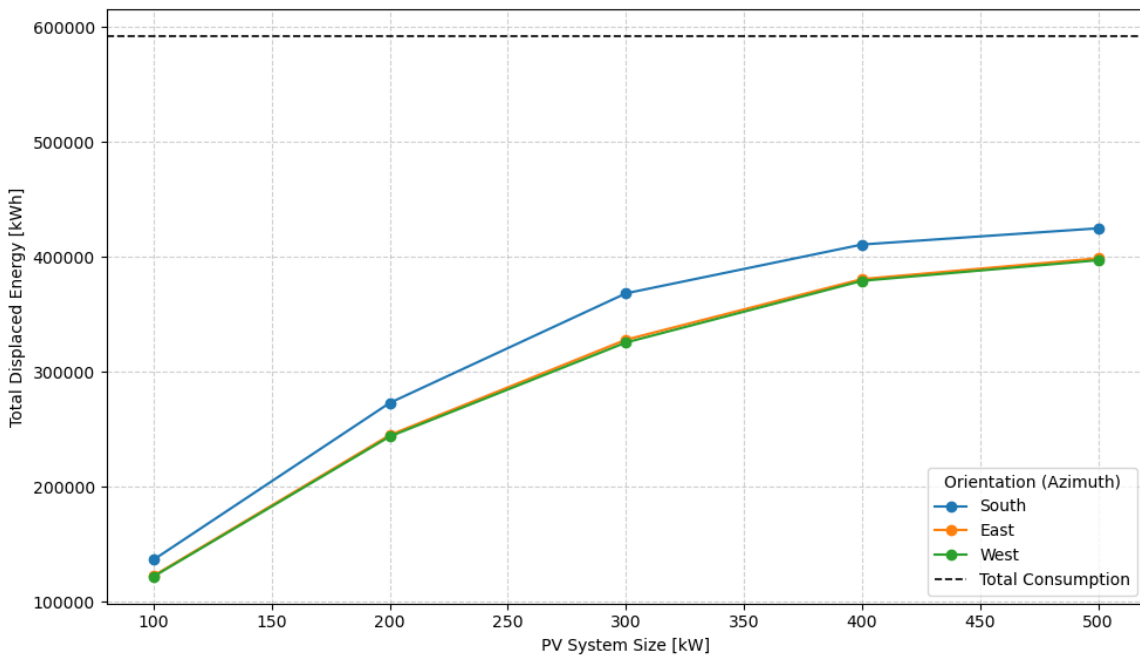


Figure 50: Growth trend of the displaced energy in Ilimanaq with increasing PV capacity.
Bifacial panels, tilt = 45°

Table 21: Annual energy output [MWh] for different system sizes and orientations.
Bifacial, 45° tilt

Scenario	100 kW	200 kW	300 kW	400 kW	500 kW
South	136.4	272.9	368.1	410.7	424.8
East	122.4	244.9	327.8	380.6	398.7
West	121.8	243.6	325.4	379.1	397.0

The behavior of the displaced energy described in Section 4.1 for 60° tilted bifacial panels is also traceable for 45° tilted bifacial panels: an initial linear increase when the capacity first doubles from 100 to 200 kW is followed by a decrease of the speed of growth, due to the reasons explained in the previous section.

The energy production plots are reported in Figures 52, 53 and 54 below.

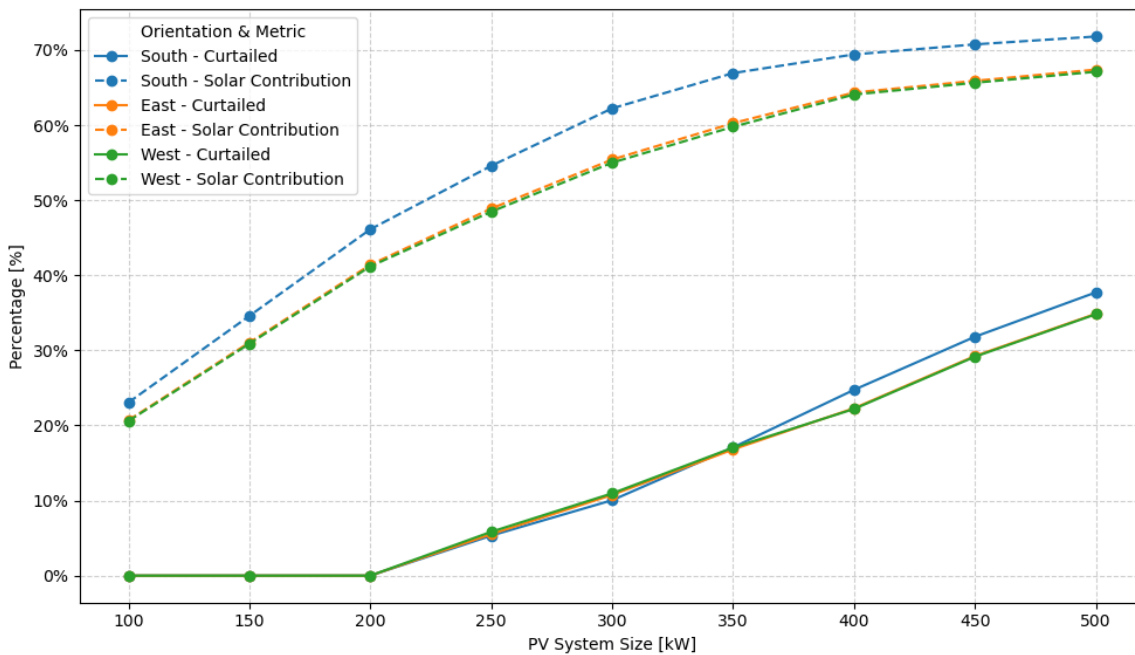


Figure 51: Growth trend of the curtailed energy in Ililamaq with increasing PV capacity.
Bifacial panels, tilt = 45°

Table 22: Curtailed Energy Percentage [%] by System Size [kW] and Orientation

Scenario	100 kW	200 kW	300 kW	400 kW	500 kW
South	0.0	0.0	10.1	24.8	37.7
East	0.0	0.0	10.8	22.3	34.9
West	0.0	0.0	11.0	22.2	34.8

Figure 51 and Table 22 also confirm the similarities between the 60° and the 45° cases. Also in this scenario, South facing panels have the smallest curtailed percentage despite the biggest production, when the plant is scaled up to 300 kW. This is again attributable to a greater share of the produced energy that gets distributed to the months with low irradiance.

The gap between West/East and South oriented panels is in this case lower than in the 60° one (1% vs. 2% difference): this small change is ascribable to the fact that the higher tilt of the previous scenario makes the panels more fit to be hit by solar radiation when the sun is low in the horizon.

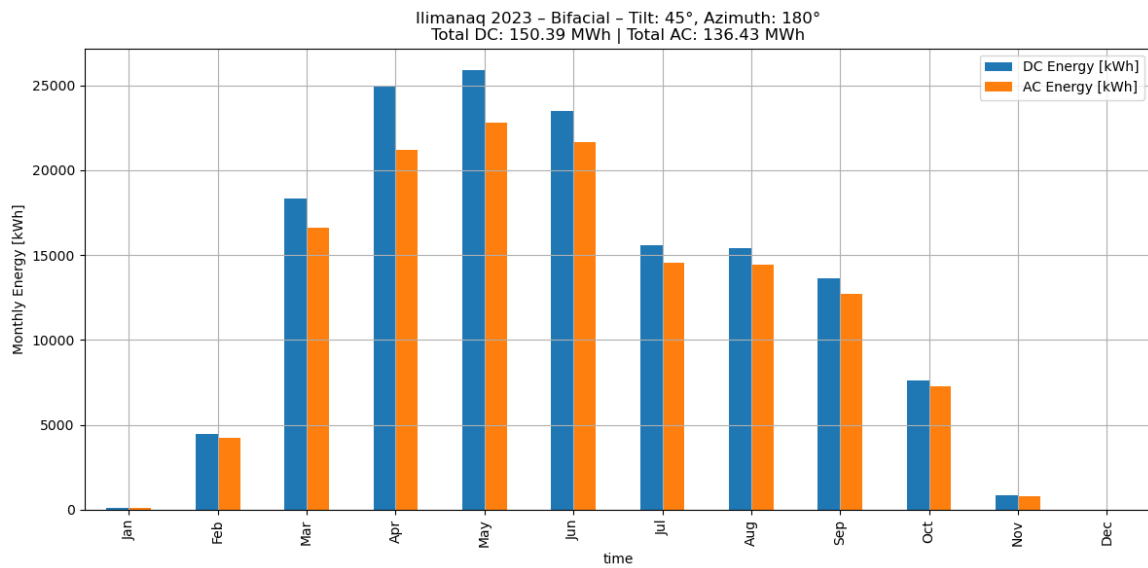


Figure 52: PV production in Ilimanaq in 2023, bifacial 100 kW plant
 Tilt = 45°, South facing

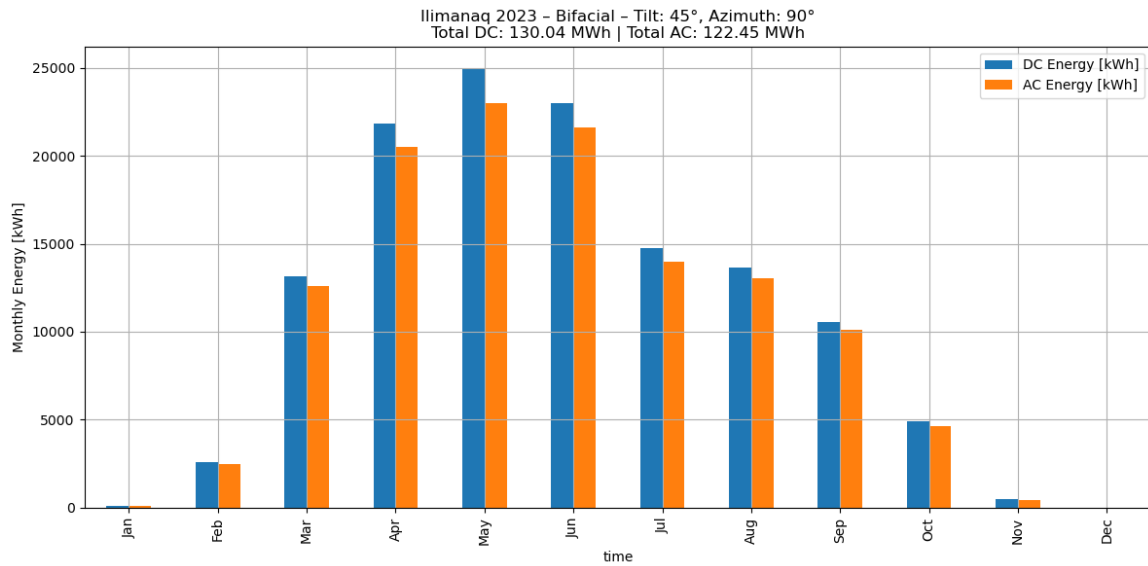


Figure 53: PV production in Ilimanaq in 2023, bifacial 100 kW plant
 Tilt = 45°, East facing

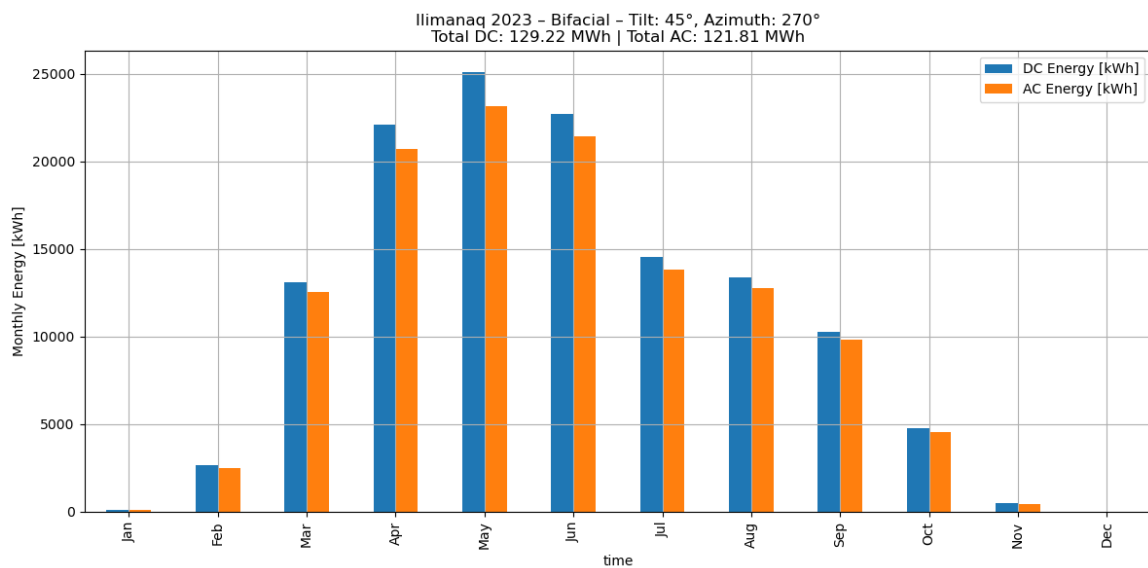


Figure 54: PV production in Ilimanaq in 2023, bifacial 100 kW plant
Tilt = 45°, West facing

H.3 Vertical bifacial panels

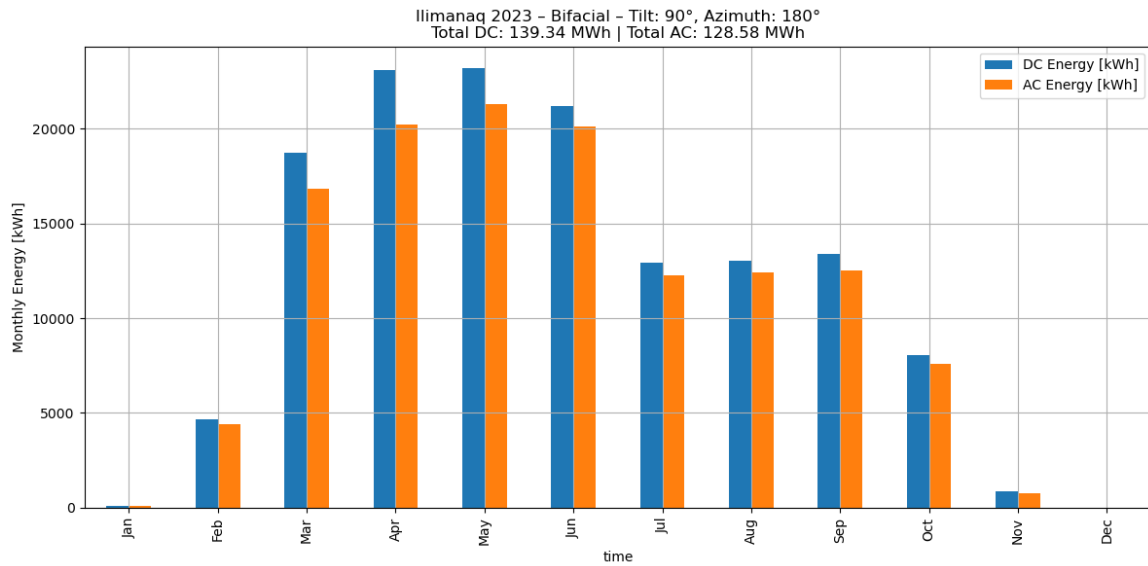


Figure 55: PV production in Ilimanaq in 2023, bifacial 100 kW plant
Vertical, South facing

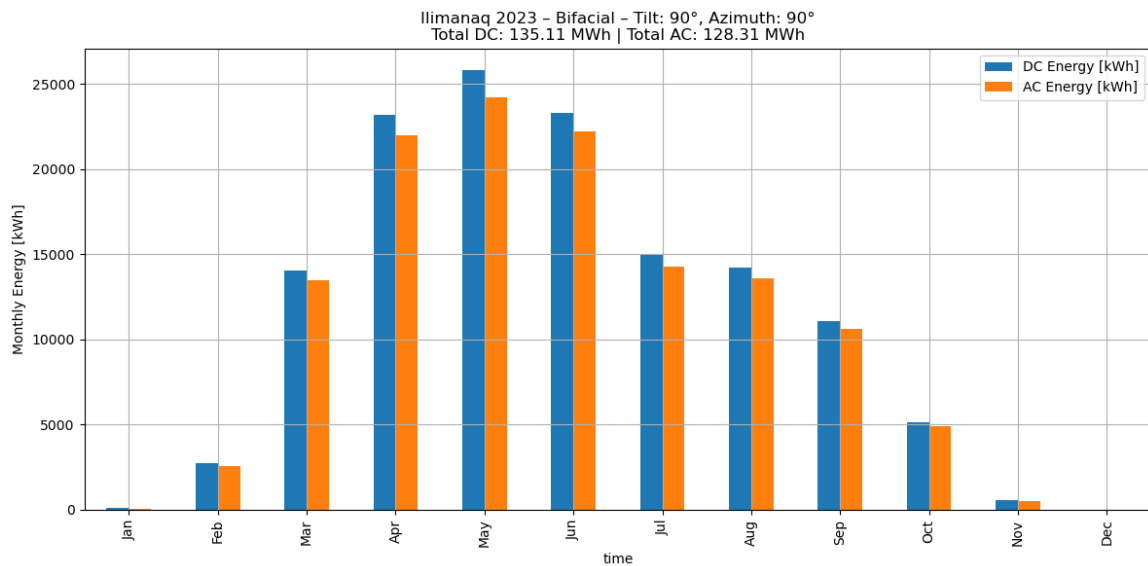


Figure 56: PV production in Ilimanaq in 2023, bifacial 100 kW plant
Vertical, East facing

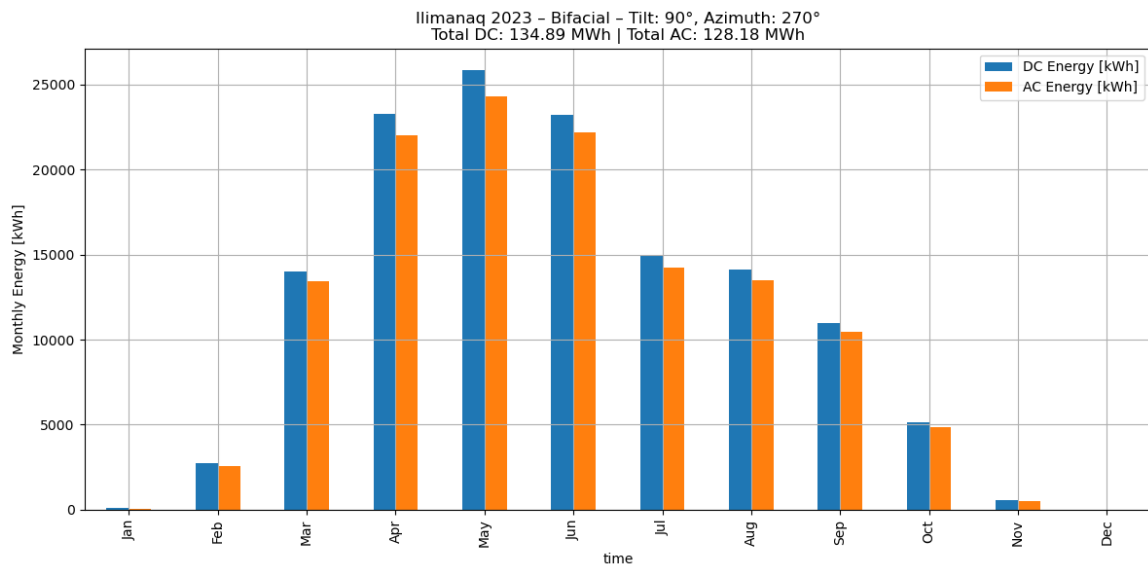


Figure 57: PV production in Ilimanaq in 2023, bifacial 100 kW plant
Vertical, West facing

H.4 Monofacial panels, 40° tilt

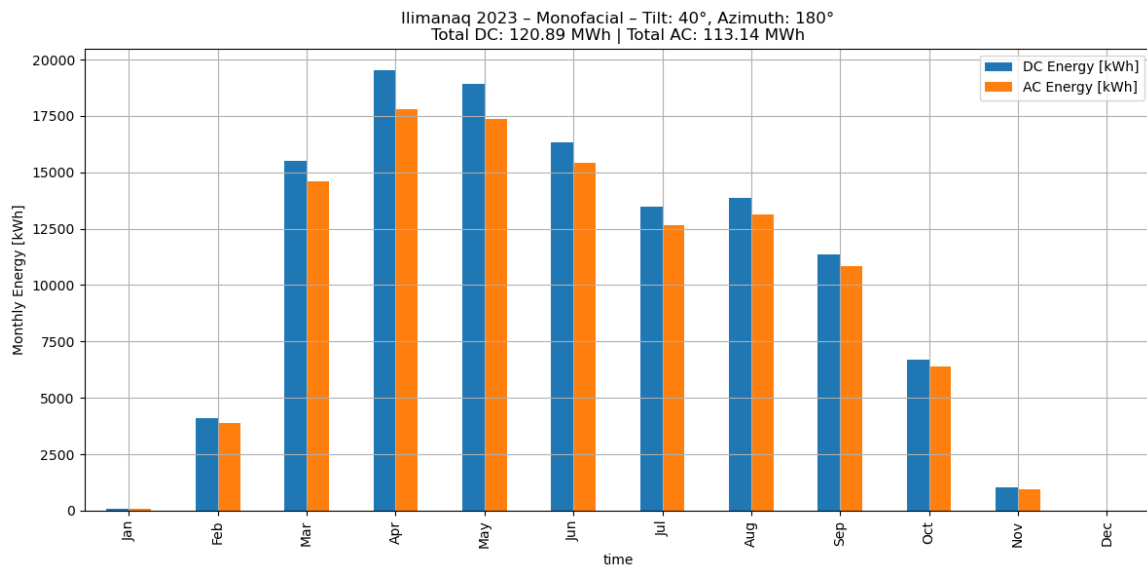


Figure 58: PV production in Ilimanaq in 2023, monofacial 100 kW plant
Tilt = 40°, South facing

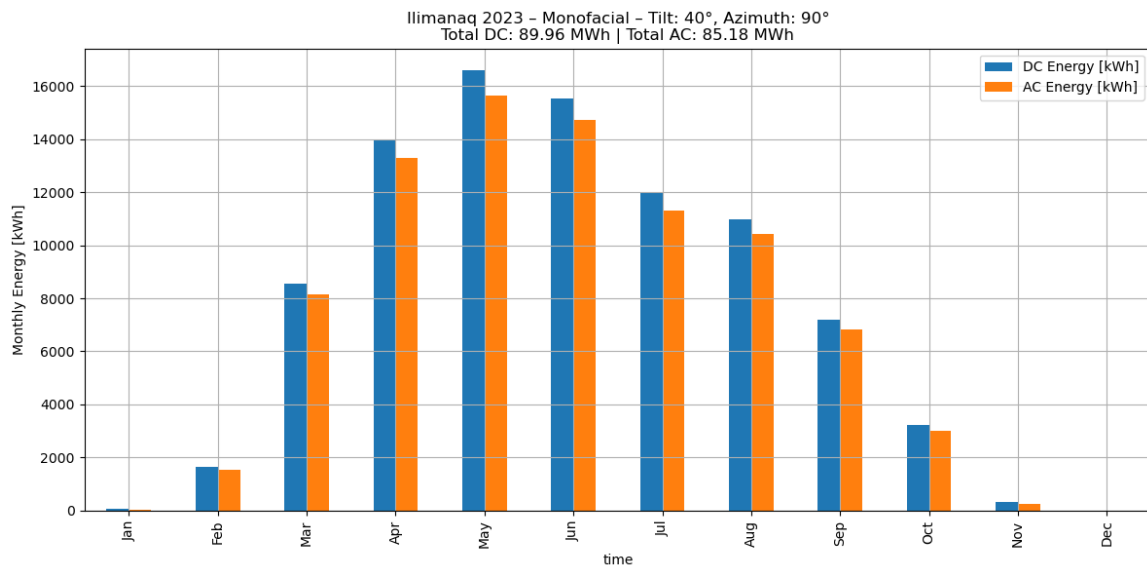


Figure 59: PV production in Ilimanaq in 2023, monofacial 100 kW plant
Tilt = 40°, East facing

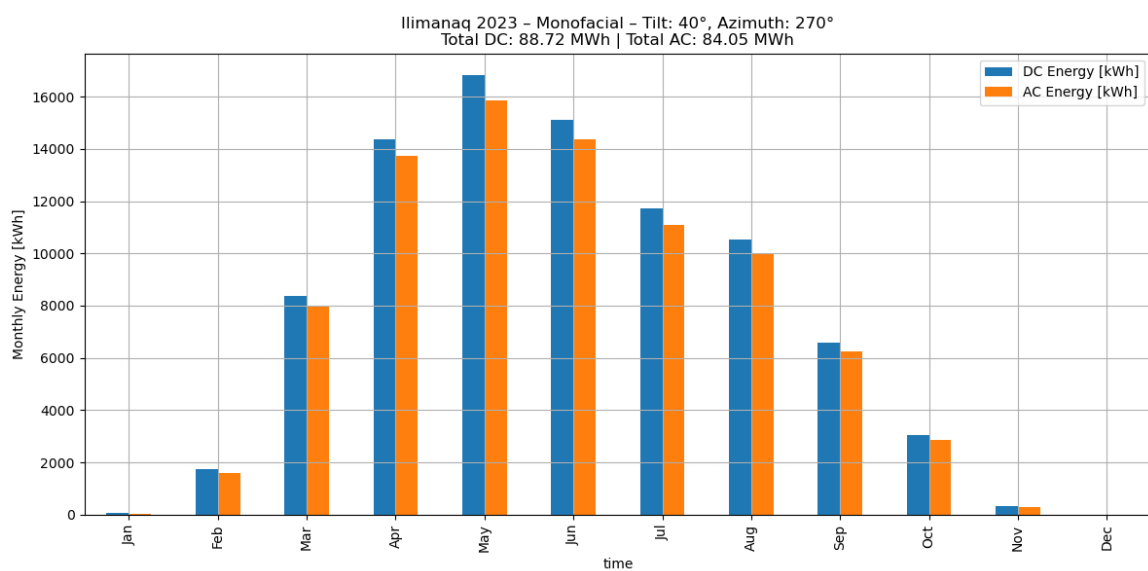


Figure 60: PV production in Ilimanaq in 2023, monofacial 100 kW plant
Tilt = 40°, West facing